

Beyond Lindblad Dynamics: Rigorous Guarantees for Thermal and Ground State Preservation under System–Bath Interactions

Ke Wang^{1,*} and Zhiyan Ding^{1,†}

¹*Department of Mathematics, University of Michigan, Ann Arbor, MI 48109, USA*

We establish new theoretical results demonstrating the efficiency and robustness of system–bath interaction models for quantum thermal and ground state preparation. Unlike existing analyses, which relies on the weak coupling Lindblad limit and require $\mathcal{O}(\text{poly}(\epsilon))$ coupling strengths for ϵ -accuracy, leading to slow mixing, we rigorously show that accurate state preparation remains possible far beyond this regime. In particular, even when the cumulative coupling strength remains constant rather than vanishing, the induced quantum channel still approximately fixes the target state. Our proof introduces new techniques for controlling all orders of the Dyson expansion and for analyzing the associated multidimensional operator Fourier transforms. These bounds substantially improve upon prior results, and numerical simulations on the TFIM and Hubbard models further confirm the robustness of the system–bath interaction framework across both weak and strong coupling regimes.

I. INTRODUCTION

Quantum thermal state and ground state preparation are fundamental primitives with broad applications in quantum many body physics, quantum chemistry, and materials science. Inspired by natural thermalization and cooling processes in open quantum systems, quantum algorithms based on dissipative dynamics have recently emerged as a powerful and efficient framework for state preparation [6, 7, 9–11, 14, 15, 18, 21, 22, 25, 29, 32, 35, 39, 40, 42, 44, 47–50]. These algorithms employ carefully engineered dissipative processes, often modeled as quantum Markov chains, to drive the system toward a desired thermal or ground state.

Within this dissipative framework, a particularly prominent approach is to employ Lindblad dynamics [16, 24]. Originally formulated as a Markovian approximation to the continuous time evolution of open quantum systems, the Lindblad equation has recently become a versatile algorithmic tool for quantum state preparation, owing to its clean and manageable mathematical structure that facilitates algorithm design. Numerous Lindblad-based works have been developed for both thermal state preparation [6, 7, 11, 35] and ground state preparation [10, 49]. This new class of Lindblad dynamics also admits efficient high-order quantum simulation algorithms [6, 8, 13, 23]. The overall simulation cost is governed by the mixing time of the underlying Lindbladian, which has been rigorously analyzed for a wide range of physically relevant models [2, 12, 19, 20, 37, 38, 45, 46, 49, 51].

One drawback of Lindblad-based algorithms is that their practical implementation often requires complex quantum operations and intricate simulation procedures. In particular, these dynamics typically involve engineering jump operators that appear as linear combinations of Heisenberg evolutions. Simulating such Lindbladians on

quantum devices therefore requires a nontrivial block-encoding of these jump operators, a process that frequently demands multiple ancilla qubits and highly structured controlled operations. These requirements pose substantial challenges for early fault-tolerant quantum devices. More recently, a different class of dissipative dynamics, the system–bath interaction framework, has been explored as a way to overcome these difficulties. In contrast to Lindbladian dynamics, this framework models the system as evolving unitarily while weakly coupled to a small ancillary bath, with dissipation arising from tracing out and resetting the bath after a prescribed duration of joint evolution. The system–bath interaction models have long been used for state preparation [1, 17, 26, 30, 34, 42, 43]. However, these works often lack rigorous performance guarantees and it can be challenging to engineer with the precision needed to reliably reach the desired target state. These difficulties have motivated a surge of recent efforts to develop system–bath interaction models that are both theoretically grounded and experimentally feasible [14, 18, 21, 25, 36]. In particular, these works propose interaction models tailored for early fault-tolerant quantum devices while offering rigorous fixed point guarantees for thermal and ground state preparation.

Although there are many ways to engineer system–bath interaction models for state preparation, theoretical analyses in the literature typically follow a common routine [14, 18, 25]. The discrete system–bath quantum channel is first approximated by an effective Lindblad evolution in the weak-coupling limit, and one then shows that the fixed point of this Lindbladian is close to the desired target state. Because this analysis relies on the validity of the weak-coupling approximation, the coupling strength must vanish with the target precision, often chosen to be $\text{poly}(\epsilon)$ in the accuracy parameter ϵ [14, 18, 25]. Such weak coupling typically leads to slow mixing of the underlying discrete quantum channel, resulting in a large number of iterations to reach the target state.

To overcome this limitation, a natural question arises:

* kwmath@umich.edu

† zyding@umich.edu

Can a system–bath interaction model prepare thermal or ground states beyond the weak coupling (Lindblad) limit?

In this work, we provide the first theoretical positive answer to this question. Our theoretical contribution is a rigorous proof that the discrete quantum channel induced by the system–bath interaction can still approximately fix the target thermal or ground state even when the cumulative coupling strength is not weak (3)—namely, beyond the traditional Lindblad limit. This surprising result substantially strengthens the theoretical understanding of the complexity of system–bath interaction models. In particular, allowing larger values of coupling coefficient enables each iteration of the algorithm to achieve a stronger contraction toward the target state, thereby reducing the total number of iterations needed for convergence. In the case of ground state preparation, our analysis removes the $\text{poly}(\epsilon)$ dependence in the iteration complexity with respect to the target precision ϵ , improving upon the prior rigorous bounds established in [14]. Beyond complexity improvements, our analysis indicates that thermalization and cooling processes within this framework may be fundamentally more robust than previously anticipated. This broader viewpoint extends beyond the conventional Lindblad description and opens new avenues for designing more efficient and experimentally feasible quantum algorithms for state preparation on near-term devices.

A second part of our contribution is illustrated through numerical tests. Building on this theoretical insight, we conduct a series of numerical tests that not only validate our analysis and demonstrate the predicted efficiency improvements, but also indicate that system–bath interaction models may perform even better in practice than suggested by our theoretical bounds. Although our theory allows the cumulative coupling strength to exceed the Lindblad limit, each iteration of the algorithm still involves a long system–bath interaction with a small coupling coefficient. Surprisingly, our numerical experiments reveal a much stronger phenomenon: even when the coupling strength per time step is $\Theta(1)$, the system–bath interaction model can still prepare the target thermal or ground state with high accuracy. This strong coupling regime lies beyond the scope of our current theoretical analysis, suggesting that system–bath interaction models may be even more efficient and robust than what our formal results presently establish.

The rest of the paper is organized as follows. In Section II, we review the system–bath interaction algorithm proposed in [14], which is the main algorithm studied in this work. In Section III, we present our main theoretical results on the fixed point property beyond the Lindblad limit. In Section IV, we provide numerical evidence that supports our theory and demonstrates improved practical efficiency. We conclude in Section V with a discussion of future research directions. A review of related literature (Appendix A) and the detailed proofs of our theoretical results are provided in Appendix.

II. SYSTEM-BATH INTERACTION ALGORITHM

We consider the system–bath interaction algorithm that was recently proposed in [14]. Given a system Hamiltonian H and inverse temperature $0 < \beta \leq \infty$, the thermal state is defined as $\sigma_\beta = e^{-\beta H}/\text{Tr}(e^{-\beta H})$, with the ground state corresponding to the limit $\beta \rightarrow \infty$. The system–bath interaction algorithm aims to prepare the target state by iteratively applying a quantum channel Φ_α generated from a system–bath interaction evolution:

$$\rho_{n+1} = \Phi_\alpha(\rho_n) := \mathbb{E} [\text{Tr}_E (U^\alpha(T) (\rho_n \otimes \rho_E) U^\alpha(T)^\dagger)] . \quad (1)$$

Here $U^\alpha(t) := \mathcal{T} \exp \left(-i \int_{-T}^t H_\alpha(s) ds \right)$ denotes the time-evolution operator of the joint system–bath dynamics up to time t . The total Hamiltonian is given by

$$H_\alpha(t) = H + H_E + \alpha f(t) \left(A_S \otimes B_E + A_S^\dagger \otimes B_E^\dagger \right) . \quad (2)$$

In the algorithm, A_S is a system coupling operator randomly chosen from a user-specified set, and it serves to induce transitions between different energy levels of the system. The environment Hamiltonian H_E is a single-qubit random Hamiltonian, and B_E is a bath coupling operator that drives transitions between the two bath energy levels. At each iteration, the environment state ρ_E is initialized to the thermal (or ground) state of H_E . The coupling strength is controlled by the parameter α together with a time-dependent control function $f(t)$. The expectation $\mathbb{E}(\cdot)$ is taken over the random choices of A_S and H_E . Although $U^\alpha(t)$ involves a time-dependent Hamiltonian simulation, the time dependence arises solely from the control function $f(t)$ and the local system–bath interaction. As a result, Eq. (1) can be efficiently implemented on *early fault-tolerant* and even *near-term* quantum devices using well-established Hamiltonian-simulation techniques [3, 4, 13, 27, 28]. The detailed simulation procedure of Φ_α can be found in [14, Section V.D].

III. MAIN RESULTS

In [14], the authors propose a choice of parameters in Eqs. (1) and (2) such that the quantum channel Φ_α can prepare the thermal or ground state of H with provable end-to-end performance guarantees within the weak-coupling (Lindblad) limit. In our work, we adopt the same choice of parameters but focus on analyzing the fixed point property of Φ_α beyond the weak coupling (Lindblad) limit. Specifically, H_E , B_E , and $f(t)$ are chosen to satisfy the following properties:

Assumption 1.

- $H_E = -\omega Z/2$, where ω is randomly sampled from a probability density $g(\omega)$.
- $B_E = (X_E - iY_E)/2 = |1\rangle\langle 0|$. A_S is uniformly sampled from a set of coupling operators $\mathcal{A} = \{A^i, -A^i\}_i$ with $\{(A^i)^\dagger\}_i = \{A^i\}_i$ and $\|A^i\| \leq 1$.

- $f(t) = \frac{1}{(2\pi)^{1/4}\sigma^{1/2}} \exp\left(-\frac{t^2}{4\sigma^2}\right)$ with $\sigma \gg 1$.

Let $\rho_{\text{fix}}(\Phi_\alpha)$ denote the fixed point of the quantum channel Φ_α and τ_{mix} be the mixing time of the quantum channel Φ_α (defined in Appendix B Definition 4). We summarize our main theoretical result below.

Theorem 2 (Informal: thermal state). *Under Assumption 1 and for any inverse temperature $\beta > 0$, we can choose $\alpha = \Theta(\sigma^{-1/2})$ and $T = \tilde{\Omega}(\sigma)$ such that $\|\rho_{\text{fix}}(\Phi_\alpha) - \sigma_\beta\|_1 = \mathcal{O}\left(\frac{\alpha^2 \beta}{\sigma} \tau_{\text{mix}}\right)$.*

Theorem 3 (Informal: ground state). *Assume H has a spectral gap Δ . Under Assumption 1 and given precision $\epsilon > 0$, we can choose $\alpha = \Theta(\sigma^{-1/2})$, $T = \tilde{\Omega}(\sigma)$, and $\sigma = \tilde{\Omega}(\Delta^{-1} \text{polylog}(\tau_{\text{mix}}/\epsilon))$ such that $\|\rho_{\text{fix}}(\Phi_\alpha) - \sigma_\beta\|_1 \leq \epsilon$.*

Here, we omit logarithmic factors in $\|H\|$, β , and $1/\epsilon$ for simplicity. The detailed statements of these theorems, along with their proofs, are provided in Appendix C and Appendix D, respectively. The mixing time τ_{mix} (defined in Appendix B Definition 4) characterizes the number of iterations needed to reach the fixed point from an arbitrary initial state.

According to Theorem 2 and Theorem 3, by choosing $\alpha = \Theta(\sigma^{-1/2})$ with sufficiently large σ , the fixed point of Φ_α can be made arbitrarily close to the target thermal or ground state, provided that the rescaled mixing time $t_{\text{mix}} := \alpha^2 \tau_{\text{mix}}$ remains bounded as σ increases. Notably, this choice of α yields a cumulative coupling strength

$$\alpha \int_{-T}^T f(t) dt = \Theta(1), \quad (3)$$

This lies beyond the traditional weak-coupling (Lindblad) regime. In contrast, previous works require $\alpha \int_{-T}^T f(t) dt = \text{poly}(\epsilon)$, as in [14, 18, 25]. In particular, [14] imposes $\alpha = \mathcal{O}(\epsilon^{1/2} \sigma^{-1})$ for both thermal and ground state preparation. We also note that [14] rigorously proves that, for several physically relevant Hamiltonians, t_{mix} remains bounded as σ increases. This implies that the number of iterations required to reach the target state scales as α^{-2} , a behavior we also verify numerically in our work, even in the regime of relatively large α (see Section IV).

Consequently, in the case when t_{mix} is upper bounded, our analysis shows that a total number of iterations $\tau_{\text{mix}} = \mathcal{O}(\sigma t_{\text{mix}})$ is sufficient to reach the target state with high accuracy. This represents a substantial improvement over the previous requirement $\tau_{\text{mix}} = \mathcal{O}(\sigma^2 \epsilon^{-1} t_{\text{mix}})$ established in [14]. In the case of ground state preparation, we obtain $\sigma = \tilde{\Omega}(\Delta^{-1} \text{polylog}(1/\epsilon))$, thereby eliminating the polynomial dependence on the target precision ϵ present in the prior bound of [14]. This is also consistent with the logarithmic dependence on ϵ achieved by high-order Lindbladian simulation algorithms [6, 8, 13, 23], while the system–bath interaction algorithm remains significantly more friendly to early fault-tolerant and even near-term quantum devices. A complexity comparison between system–bath interaction and

Lindblad-dynamics–based algorithms is provided in Appendix E.

Finally, we note that our numerical results in Section IV suggest that the condition $\alpha\sqrt{\sigma} = \Theta(1)$ might be further relaxed to $\alpha/\sqrt{\sigma} = \Theta(1)$. In our current proof, this requirement is needed to ensure that each term in the Dyson series expansion remains norm-bounded. The detailed argument is given in Appendix C and Appendix D. Understanding how to weaken this condition while maintaining rigorous guarantees is an interesting direction for future work.

IV. NUMERICAL RESULTS

Our numerical experiments validate our theoretical results and assess the practical performance of the system–bath interaction algorithm on three representative models: the transverse-field Ising model (TFIM), the Hubbard model, and 1D axial next-nearest-neighbor Ising (ANNNI) model. We investigate both thermal state and ground state preparation for the first two models and only ground state for the last model, varying the coupling parameter α to examine its impact on convergence behavior and accuracy. In our tests, we focus on two properties of the quantum channel Φ_α :

- Dynamics of density operator/state: We simulate the iterative application of the quantum channel Φ_α on an initial state ρ_0 and track the evolution of fidelity (for thermal and ground states) or energy (only for ground states) over iterations along a single trajectory. This allows us to observe how quickly the state converges to the target state under different choices of α and σ .
- Fixed point and spectral gap analysis: We numerically calculate the quantum channel Φ_α as a superoperator and compute its fixed point and spectral gap. This enables us to quantify the accuracy of the fixed point in approximating the target state and to assess the mixing time of the channel under various parameter settings.

For both models, we not only verify our theoretical predictions in the regime $\alpha\sqrt{\sigma} = \Theta(1)$ but also explore the stronger-coupling regime where $\alpha/\sqrt{\sigma} = \Theta(1)$, corresponding to large system–bath interaction strength per time step.

a. *Transverse field Ising model (TFIM) beyond Lindblad limit:* We first consider the transverse field Ising model (TFIM) with $L = 4, 8$ sites:

$$H = -J \sum_{i=1}^{L-1} Z_i Z_{i+1} - g \sum_{i=1}^L X_i, \quad (4)$$

where g is the coupling coefficient, Z_i, X_i are Pauli operators for the i th site and the dimension of H is 2^L . We set $J = 1, g = 1.2$. Here, we present the result of the thermal

state preparation with $\alpha\sqrt{\sigma} = \Theta(1)$ and $L = 4$. Similar numerical results for ground state preparation and $L = 8$ are provided in Appendix F 1.

For the thermal state case, we sample A_S uniformly chosen from the single-qubit Pauli set, with positive and negative signs assigned with equal probability. The results are shown in Fig. 1 (with more detailed results in Appendix F 1 Fig. 4). In the first figure of Fig. 1, we fix $\sigma = 1$ and vary α to examine the convergence behavior of the fidelity in the algorithm, which is defined as $F(\rho, \sigma_\beta) = \left(\text{Tr} \sqrt{\sqrt{\sigma_\beta} \rho \sqrt{\sigma_\beta}} \right)^2$. It can be clearly observed that when $\alpha\sqrt{\sigma} = \Theta(1)$, the state converges to the thermal state, and the convergence speed increases as α grows. This matches with our theoretical results in Theorem 2. Next, we explicitly construct the quantum channel Φ_α and numerically compute its spectral gap, as shown in the second figure of Fig. 1. From Appendix F 1 and Fig. 4b, we observe that as σ increases, the steady state of Φ_α approaches the target thermal state more closely. Moreover, the spectral gap of Φ_α remains independent of σ and scales as α^2 . Since the mixing time is inversely proportional to the spectral gap, this implies that τ_{mix} scales as α^{-2} , and therefore larger choices of α lead to faster convergence.

b. Hubbard model beyond Lindblad limit: Consider the 1-D Hubbard model defined on $L = 2, 4$ spinful sites with open boundary conditions

$$H = -t \sum_{j=1}^{L-1} \sum_{\sigma \in \{\uparrow, \downarrow\}} c_{j,\sigma}^\dagger c_{j+1,\sigma} + U \sum_{j=1}^L \left(n_{j,\uparrow} - \frac{1}{2} \right) \left(n_{j,\downarrow} - \frac{1}{2} \right). \quad (5)$$

where the number operator $n_{j,\sigma} = c_{j,\sigma}^\dagger c_{j,\sigma}$ and the dimension is 2^{2L} . We choose $t = 1$, $U = -4$, and A_S is uniformly sampled from $\mathcal{A} = \left\{ \pm c_{j,\sigma}, \pm c_{j,\sigma}^\dagger \right\}_{j=1, \dots, L, \sigma=\uparrow, \downarrow}$. Similar to the TFIM case, we consider both the thermal state and the ground state case with the same choice of parameters and observe similar results. Here, we present the result of the ground state preparation with $L = 2$ (4 qubits) in Fig. 2 and leave the thermal state results in Appendix F 2.

c. TFIM/Hubbard/ANNNI model with strong coupling: For both models, we investigate the stronger-coupling regime where $\alpha/\sqrt{\sigma} = \Theta(1)$. Here, we present the result with TFIM-8 and Hubbard-4 (8 qubits) with the same parameters as in (4) and (5), except that we set $\alpha = c\sqrt{\sigma}$ with $0.03 \leq c \leq 5$. The results are shown in Fig. 3, where $\alpha/\sqrt{\sigma}$. The results with 4 qubits can be found in Appendix F 1 Fig. 6 and Appendix F 2 Fig. 9, respectively. In addition, the result with ground state in TFIM-8 and Hubbard-4 are provided in Appendix F 4.

Remarkably, even in this strong-coupling regime ($\alpha/\sqrt{\sigma} \approx 0.5$), the system-bath interaction model still prepares the target thermal or ground state with high accuracy, and the convergence speed increases as α grows. Furthermore, the apparent coupling threshold at $\alpha/\sqrt{\sigma} \approx 0.5$ seems to be independent of system size, as

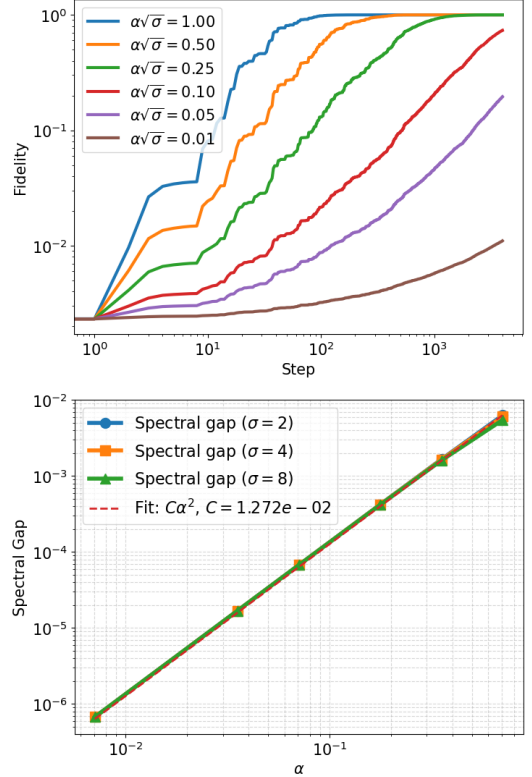


Figure 1: Numerical results for thermal state preparation of TFIM with $L = 4$ sites in the regime $\alpha\sqrt{\sigma} = \Theta(1)$. We set $\beta = 1$, $\sigma = 2, 4, 8$, $\sqrt{2}\alpha = 1, 0.5, 0.25, 0.1, 0.05, 0.01$, and $T = 5\sigma$. The frequency ω is uniformly sampled from the interval $[0, 5]$. Upper: evolution of fidelity; Lower: spectral gap of Φ_α .

we observe similar behavior in both 4-qubit and 8-qubit systems. This phenomenon lies beyond our current theoretical guarantees and suggests that the robustness of system-bath interaction models may be even greater than what our analysis presently establishes.

Finally, we test the performance of our algorithm for preparing the ground state of 1D axial next-nearest-neighbor Ising (ANNNI) model [41]. In [49], it was shown that preparing the ground state of H_{ANNNI} via adiabatic evolution is challenging, as the effective spectral gap closes multiple times along the adiabatic path if the initial Hamiltonian is set to be $H_0 = -Z$. In our work, we evaluate the performance of our ground state preparation algorithm on this model with the same choice of parameters as that in the case of TFIM or Hubbard models (See detail in Appendix F 3). We continue to observe clear convergence, along with a consistent relationship between the spectral gap and α^2 , mirroring the behavior seen in the TFIM and Hubbard models; see Appendix F 3 and Fig. 10.

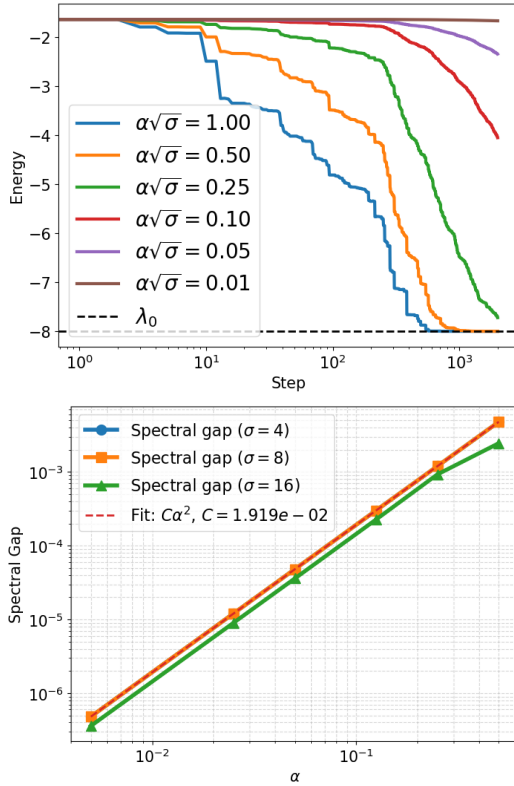


Figure 2: Numerical results for ground state preparation of the Hubbard model with $L = 2$ sites in the regime $\alpha\sqrt{\sigma} = \Theta(1)$. We set $\alpha = 0.5, 0.25, 0.125, 0.05, 0.025, 0.005$, $\sigma = 4, 8, 16$, $T = 5\sigma$, and also sample ω uniformly from $[0, 5]$. Upper: evolution of energy, λ_0 is the ground state energy; Lower: spectral gap of Φ_α .

V. CONCLUSION AND OUTLOOK

In this work, we have theoretically demonstrated that system–bath interaction models can prepare thermal and ground states beyond the traditional weak-coupling (Lindblad) limit. We prove that, when the cumulative interaction strength per iteration is $\Theta(1)$, the fixed point of the induced quantum channel can still closely approximate the target state. This result substantially broadens the theoretical understanding of system–bath interaction frameworks and significantly improves the previous rigorous performance guarantees for dissipative state preparation algorithms. Conceptually, it suggests that thermalization and cooling processes may be far more robust than previously anticipated, opening new avenues for designing more efficient quantum state preparation algorithms suitable for near-term devices.

Beyond our theoretical results, several promising directions remain for future research. First, our numerical experiments suggest that system–bath interaction models may perform even better in practice than our cur-

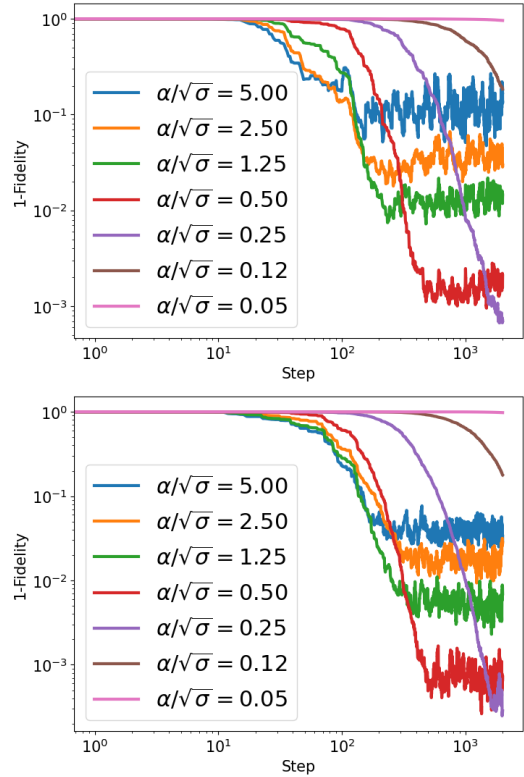


Figure 3: Evolution of infidelity for thermal state preparation with $\alpha/\sqrt{\sigma} = \Theta(1)$. Upper: TFIM with $L = 8$ sites; Lower: Hubbard model with $L = 4$ sites.

rent bounds indicate, particularly in the strong-coupling regime where the per-step coupling strength is $\Theta(1)$. Developing a theoretical understanding of this regime is an important open problem and may further clarify the robustness and efficiency of these algorithms. Second, although our analysis focuses on a specific system–bath interaction model, it would be possible and valuable to extend our techniques to other models in the literature and to investigate their fixed point properties beyond the Lindblad limit. Third, although our numerical simulations on small-scale systems confirm both our theoretical predictions and the fast-mixing behavior, developing a theoretical understanding of the mixing time in larger and more general systems remains an open problem. This is a necessary step toward establishing comprehensive end-to-end performance guarantees for system–bath interaction algorithms, such as those in [14]. Since the discrete quantum channel in our setting is no longer close to a Lindblad evolution, new analytical techniques will be required to analyze its mixing properties. Developing such tools lies beyond the scope of the present work and represents an important direction for future research. Finally, our work primarily varies the coupling parameter α while keeping σ large to ensure accurate fixed point approximation. While large σ improves accuracy, it also increases the required interaction time T and thus the

per-iteration implementation cost. An interesting question is whether one can further reduce the dependence on σ while maintaining good performance, analogous to the improvement achieved in [7] over [6] in the context of Lindbladian dynamics.

Acknowledgments— This work was supported in part by the University of Michigan through a startup grant (Z.D.). The authors thank Yongtao Zhan, Lin Lin for helpful discussions.

[1] Trond I Andersen, Nikita Astrakhantsev, Amir H Karamlou, Julia Berndtsson, Johannes Motruk, Aaron Szasz, Jonathan A Gross, Alexander Schuckert, Tom Westerhout, Yaxing Zhang, et al. Thermalization and criticality on an analogue–digital quantum simulator. *Nature*, 638(8049):79–85, 2025.

[2] Ivan Bardet, Ángela Capel, Li Gao, Angelo Lucia, David Pérez-García, and Cambyses Rouzé. Rapid thermalization of spin chain commuting Hamiltonians. *Phys. Rev. Lett.*, 130(6):060401, 2023.

[3] Dominic W Berry, Graeme Ahokas, Richard Cleve, and Barry C Sanders. Efficient quantum algorithms for simulating sparse Hamiltonians. *Commun. Math. Phys.*, 270:359–371, 2007.

[4] Dominic W Berry, Andrew M Childs, Richard Cleve, Robin Kothari, and Rolando D Somma. Exponential improvement in precision for simulating sparse Hamiltonians. In *STOC 2014*, 2014.

[5] Chi-Fang Chen and Fernando G. S. L. Brandão. Fast thermalization from the eigenstate thermalization hypothesis. *arXiv:2112.07646*, 2023.

[6] Chi-Fang Chen, Michael J Kastoryano, Fernando GSL Brandão, and András Gilyén. Quantum thermal state preparation. *arXiv:2303.18224*, 2023.

[7] Chi-Fang Chen, Michael J Kastoryano, and András Gilyén. An efficient and exact noncommutative quantum Gibbs sampler. *arXiv:2311.09207*, 2023.

[8] Richard Cleve and Chunhao Wang. Efficient quantum algorithms for simulating Lindblad evolution. In *ICALP 2017*, volume 80, pages 17:1–17:14, 2017.

[9] Toby S. Cubitt. Dissipative ground state preparation and the dissipative quantum eigensolver. *arXiv:2303.11962*, 2023.

[10] Zhiyan Ding, Chi-Fang Chen, and Lin Lin. Single-ancilla ground state preparation via Lindbladians. *Phys. Rev. Research*, 6:033147, 2024.

[11] Zhiyan Ding, Bowen Li, and Lin Lin. Efficient quantum Gibbs samplers with Kubo–Martin–Schwinger detailed balance condition. *Commun. Math. Phys.*, 406(3):67, 2025.

[12] Zhiyan Ding, Bowen Li, Lin Lin, and Ruizhe Zhang. Polynomial-time preparation of low-temperature Gibbs states for 2D Toric Code. *arXiv:2410.01206*, 2024.

[13] Zhiyan Ding, Xiantao Li, and Lin Lin. Simulating open quantum systems using Hamiltonian simulations. *PRX Quantum*, 5:020332, 2024.

[14] Zhiyan Ding, Yongtao Zhan, John Preskill, and Lin Lin. End-to-end efficient quantum thermal and ground state preparation made simple. *arXiv:2508.05703*, 2025.

[15] András Gilyén, Chi-Fang Chen, Joao F. Doriguello, and Michael J. Kastoryano. Quantum generalizations of Glauber and Metropolis dynamics. *arXiv:2405.20322*, 2024.

[16] Vittorio Gorini, Andrzej Kossakowski, and Ennackal Chandy George Sudarshan. Completely positive dynamical semigroups of n -level systems. *J. Math. Phys.*, 17:821–825, 1976.

[17] Matthew Hagan and Nathan Wiebe. The thermodynamic cost of ignorance: Thermal state preparation with one ancilla qubit. *arXiv:2502.03410*, 2025.

[18] Dominik Hahn, S. A. Parameswaran, and Benedikt Placke. Provably efficient quantum thermal state preparation via local driving. *arXiv:2505.22816*, 2025.

[19] Michael J Kastoryano and Kristan Temme. Quantum logarithmic Sobolev inequalities and rapid mixing. *J. Math. Phys.*, 54(5):1–34, 2013.

[20] Jan Kochanowski, Alvaro M Alhambra, Angela Capel, and Cambyses Rouzé. Rapid thermalization of dissipative many-body dynamics of commuting Hamiltonians. *Commun. Math. Phys.*, 2024.

[21] Josias Langbehn, George Mouloudakis, Emma King, Raphaël Menu, Igor Gornyi, Giovanna Morigi, Yuval Gefen, and Christiane P. Koch. Universal cooling of quantum systems via randomized measurements. *arXiv:2506.11964*, 2025.

[22] Hao-En Li, Yongtao Zhan, and Lin Lin. Dissipative ground state preparation in ab initio electronic structure theory. *arXiv:2411.01470*, 2024.

[23] Xiantao Li and Chunhao Wang. Simulating Markovian open quantum systems using higher-order series expansion. In *ICALP 2023*, volume 261, pages 87:1–87:20, 2023.

[24] Goran Lindblad. On the generators of quantum dynamical semigroups. *Commun. Math. Phys.*, 48:119–130, 1976.

[25] Jerome Lloyd and Dmitry A. Abanin. Quantum thermal state preparation for near-term quantum processors. *arXiv:2506.21318*, 2025.

[26] Jerome Lloyd, Alexios A. Michailidis, Xiao Mi, Vadim Smelyanskiy, and Dmitry A. Abanin. Quasiparticle cooling algorithms for quantum many-body state preparation. *PRX Quantum*, 6:010361, March 2025.

[27] Guang Hao Low and Isaac L. Chuang. Optimal Hamiltonian simulation by quantum signal processing. *Phys. Rev. Lett.*, 118:010501, 2017.

[28] Guang Hao Low and Isaac L. Chuang. Hamiltonian Simulation by Qubitization. *Quantum*, 3:163, 2019.

[29] Tsung-Cheng Lu, Leonardo A Lessa, Isaac H Kim, and Timothy H Hsieh. Measurement as a shortcut to long-range entangled quantum matter. *PRX Quantum*, 3(4):040337, 2022.

[30] X. Mi, A. A. Michailidis, S. Shabani, K. C. Miao, P. V. Klimov, J. Lloyd, E. Rosenberg, R. Acharya, I. Aleiner, T. I. Andersen, M. Ansmann, F. Arute, K. Arya, A. Asfaw, J. Atalaya, J. C. Bardin, A. Bengtsson, G. Bortoli, A. Bourassa, J. Bovaird, L. Brill, M. Broughton, B. B. Buckley, D. A. Buell, T. Burger, B. Burkett, N. Bushnell, Z. Chen, B. Chiaro, D. Chik, C. Chou, J. Co

gan, R. Collins, P. Conner, W. Courtney, A. L. Crook, B. Curtin, A. G. Dau, D. M. Debroy, A. Del Toro Barba, S. Demura, A. Di Paolo, I. K. Drozdov, A. Dunsworth, C. Erickson, L. Faoro, E. Farhi, R. Fatemi, V. S. Ferreira, L. F. Burgos, E. Forati, A. G. Fowler, B. Foxen, É. Genois, W. Giang, C. Gidney, D. Gilboa, M. Giustina, R. Gosula, J. A. Gross, S. Habegger, M. C. Hamilton, M. Hansen, M. P. Harrigan, S. D. Harrington, P. Heu, M. R. Hoffmann, S. Hong, T. Huang, A. Huff, W. J. Huggins, L. B. Ioffe, S. V. Isakov, J. Iveland, E. Jeffrey, Z. Jiang, C. Jones, P. Juhas, D. Kafri, K. Kechedzhi, T. Khattar, M. Khezri, M. Kieferová, S. Kim, A. Kitaev, A. R. Klots, A. N. Korotkov, F. Kostritsa, J. M. Kreikebaum, D. Landhuis, P. Laptev, K.-M. Lau, L. Laws, J. Lee, K. W. Lee, Y. D. Lensky, B. J. Lester, A. T. Lill, W. Liu, A. Locharla, F. D. Malone, O. Martin, J. R. McClean, M. McEwen, A. Mieszala, S. Montazeri, A. Morvan, R. Movassagh, W. Mruczkiewicz, M. Neeley, C. Neill, A. Nersisyan, M. Newman, J. H. Ng, A. Nguyen, M. Nguyen, M. Y. Niu, T. E. O'Brien, A. Opremcak, A. Petukhov, R. Potter, L. P. Pryadko, C. Quintana, C. Rocque, N. C. Rubin, N. Saei, D. Sank, K. Sankaragomathi, K. J. Satzinger, H. F. Schurkus, C. Schuster, M. J. Shearn, A. Shorter, N. Shutty, V. Shvarts, J. Skrzyni, W. C. Smith, R. Somma, G. Sterling, D. Strain, M. Szałay, A. Torres, G. Vidal, B. Villalonga, C. V. Heidweiller, T. White, B. W. K. Woo, C. Xing, Z. J. Yao, P. Yeh, J. Yoo, G. Young, A. Zalcman, Y. Zhang, N. Zhu, N. Zobrist, H. Neven, R. Babbush, D. Bacon, S. Boixo, J. Hilton, E. Lucero, A. Megrant, J. Kelly, Y. Chen, P. Roushan, V. Smelyanskiy, and D. A. Abanin. Stable quantum-correlated many-body states through engineered dissipation. *Science*, 383(6689):1332–1337, 2024.

[31] Daniel Molpeceres, Sirui Lu, J. Ignacio Cirac, and Barbara Kraus. Quantum algorithms for cooling: a simple case study. *arXiv:2503.24330*, 2025.

[32] Evgeny Mozgunov and Daniel Lidar. Completely positive master equation for arbitrary driving and small level spacing. *Quantum*, 4:227, February 2020.

[33] We note that [6] focuses exclusively on the thermal state preparation setting. Nevertheless, one can derive a fixed point error bound for ground state preparation analogous to that in [14] for the dynamics in (E4). Consequently, the parameter σ should be chosen in the same scaling.

[34] Stefano Polla, Yaroslav Herasymenko, and Thomas E. O'Brien. Quantum digital cooling. *Phys. Rev. A*, 104:012414, Jul 2021.

[35] Patrick Rall, Chunhao Wang, and Paweł Wocjan. Thermal state preparation via rounding promises. *Quantum*, 7:1132, 2023.

[36] Carlos Ramon-Escandell, Alessandro Prosinotto, and Dvira Segal. Thermal state preparation by re-peated interactions at and beyond the Lindblad limit. *arXiv:2506.12166*, 2025.

[37] Cambyses Rouzé, Daniel Stilck França, and Álvaro M Alhambra. Optimal quantum algorithm for Gibbs state preparation. *arXiv:2411.04885*, 2024.

[38] Cambyses Rouzé, Daniel Stilck França, and Álvaro M. Alhambra. Efficient thermalization and universal quantum computing with quantum gibbs samplers. In *STOC 25*, page 1488–1495, 2025.

[39] Sthitadhi Roy, JT Chalker, IV Gornyi, and Yuval Gefen. Measurement induced steering of quantum systems. *Phys. Rev. Research*, 2(3):033347, 2020.

[40] Matteo Scandi and Álvaro M. Alhambra. Thermalization in open many-body systems and KMS detailed balance. *arXiv:2505.20064*, 2025.

[41] Walter Selke. The anni model-theoretical analysis and experimental application. *Physics Reports*, 170(4):213–264, 1988.

[42] Oles Shtanko and Ramis Movassagh. Preparing thermal states on noiseless and noisy programmable quantum processors. *arXiv:2112.14688*, 2021.

[43] Hong-Yi Su and Ying Li. Quantum algorithm for the simulation of open-system dynamics and thermalization. *Phys. Rev. A*, 101:012328, Jan 2020.

[44] K. Temme, T. J. Osborne, K. G. Vollbrecht, D. Poulin, and F. Verstraete. Quantum Metropolis sampling. *Nature*, 471(7336):87–90, March 2011.

[45] Kristan Temme, Michael James Kastoryano, Mary Beth Ruskai, Michael Marc Wolf, and Frank Verstraete. The χ^2 -divergence and mixing times of quantum Markov processes. *J. Math. Phys.*, 51(12), 2010.

[46] Yu Tong and Yongtao Zhan. Fast mixing of weakly interacting fermionic systems at any temperature. *PRX Quantum*, 6:030301, Jul 2025.

[47] Frank Verstraete, Michael M. Wolf, and I. Cirac. Quantum computation and quantum-state engineering driven by dissipation. *Nat. Phys.*, 5(9):633–636, 2009.

[48] Yunzhao Wang, Kyrylo Snizhko, Alessandro Romito, Yuval Gefen, and Kater Murch. Dissipative preparation and stabilization of many-body quantum states in a superconducting qutrit array. *Phys. Rev. A*, 108:013712, 2023.

[49] Yongtao Zhan, Zhiyan Ding, Jakob Huhn, Johnnie Gray, John Preskill, Garnet Kin-Lic Chan, and Lin Lin. Rapid quantum ground state preparation via dissipative dynamics. *arXiv:2503.15827*, 2025.

[50] Leo Zhou, Soonwon Choi, and Mikhail D Lukin. Symmetry-protected dissipative preparation of matrix product states. *Phys. Rev. A*, 104(3):032418, 2021.

[51] Štěpán Šmíd, Richard Meister, Mario Berta, and Roberto Bondesan. Polynomial time quantum Gibbs sampling for Fermi-Hubbard model at any temperature. *arXiv:2501.01412*, 2025.

Appendix A: Related works

In the literature, there is a vast of work on dissipation quantum algorithms for thermal and ground state preparation [6, 7, 9–11, 14, 15, 18, 21, 22, 25, 29, 32, 35, 39, 40, 42, 44, 47–50]. Because our paper mainly focuses on the system-bath interaction model, we will mainly review the works that are closely related to ours in this section.

Recently, several system-bath-interaction-based algorithms have been proposed for thermal state preparation [5, 14, 17, 18, 21, 25, 31, 40]. While these works share a broadly similar algorithmic structure, they differ in the choice of bath model and in the design of the system-bath interaction. Their theoretical analyses also follow a common

pattern, as discussed in Section I: one first approximates the discrete system–bath quantum channel by an effective Lindblad evolution in the weak-coupling limit, and then shows that the fixed point of this Lindbladian is close to the desired target state.

However, because this approach relies critically on the weak-coupling approximation, these methods typically require the coupling strength to vanish with the target precision, often chosen to be polynomially small in the accuracy parameter ϵ [14, 18, 25]. This, in turn, leads to slow mixing of the underlying discrete quantum channel and consequently demands a large number of iterations to reach the target state. Our work departs from this paradigm by directly analyzing the fixed point properties of the discrete quantum channel beyond the weak-coupling limit. This allows us to choose larger coupling strengths, thereby accelerating convergence to the target state and improving overall algorithmic efficiency. It is worth noting that the non-vanishing coupling-strength regime has also been explored in [36], where the authors theoretically study a special three-level system-bath interaction model and numerically investigate a repeated interaction model for thermal and ground-state preparation under moderate coupling strength. However, for general Hamiltonians H , a rigorous theoretical characterization of the fixed-point property in this regime remains open.

Appendix B: Notations and preliminaries

For a matrix $A \in \mathbb{C}^{N \times N}$, let A^* , A^T , and A^\dagger denote the complex conjugate, transpose, and Hermitian transpose (adjoint), respectively. The Schatten p -norm is defined as

$$\|A\|_p = \text{Tr} \left(\left(\sqrt{A^\dagger A} \right)^p \right)^{1/p}.$$

The Schatten 1-norm $\|A\|_1$ is the trace norm; the Schatten 2-norm $\|A\|_2$ is the Hilbert–Schmidt norm (or Frobenius norm for matrices); and the Schatten ∞ -norm $\|A\|_\infty$ coincides with the operator norm $\|A\|$. For a superoperator $\Phi : \mathbb{C}^{N \times N} \rightarrow \mathbb{C}^{N \times N}$, we define the induced trace norm

$$\|\Phi\|_{1 \leftrightarrow 1} = \sup_{\|A\|_1=1} \|\Phi(A)\|_1.$$

Let $\{|\psi_i\rangle\}$ be the eigenstates of a Hamiltonian H with eigenvalues $\{\lambda_i\}$. Each difference $\lambda_i - \lambda_j$ is called a *Bohr frequency*, and we denote by $B(H)$ the set of all Bohr frequencies. For $\nu \in B(H)$ and an operator A , we define

$$A(\nu) = \sum_{\lambda_j - \lambda_i = \nu} |\psi_j\rangle \langle \psi_j| A |\psi_i\rangle \langle \psi_i|, \quad (\text{B1})$$

where $|\psi_i\rangle$ is the eigenvector of H with eigenvalue λ_i .

We define the mixing time of a discrete quantum channel as follows.

Definition 4. Let Φ be a CPTP map with a unique fixed point $\rho_{\text{fix}}(\Phi)$ and let $\epsilon > 0$. The integer mixing time $\tau_{\text{mix},\Phi}$ is

$$\tau_{\text{mix},\Phi} = \min \left\{ t \in \mathbb{N} \left| \sup_{\rho_1 \neq \rho_2} \frac{\|\Phi^t(\rho_1) - \Phi^t(\rho_2)\|_1}{\|\rho_1 - \rho_2\|_1} \leq \frac{1}{2} \right. \right\}. \quad (\text{B2})$$

For channels of the form (1), the parameter α^2 plays the role of an effective contraction time per iteration, and we define the rescaled mixing time

$$t_{\text{mix},\Phi} = \alpha^2 \tau_{\text{mix},\Phi}. \quad (\text{B3})$$

This definition is stronger than the one used in [14], where mixing time is defined in terms of convergence to the fixed point and depends explicitly on the target precision ϵ . Our results can be extended to that weaker definition with minor modifications; for simplicity, we work with Definition 4.

We adopt the following asymptotic notations besides the usual big- \mathcal{O} notation. We write $f = \Omega(g)$ if $g = \mathcal{O}(f)$, and $f = \Theta(g)$ if both $f = \mathcal{O}(g)$ and $g = \mathcal{O}(f)$. The notations $\tilde{\mathcal{O}}$, $\tilde{\Omega}$, and $\tilde{\Theta}$ suppress only subdominant polylogarithmic factors: unless otherwise specified,

$$f = \tilde{\mathcal{O}}(g) \iff f = \mathcal{O}(g \text{ polylog}(g)), \quad f = \tilde{\Omega}(g) \iff f = \Omega(g \text{ polylog}(g)), \quad f = \tilde{\Theta}(g) \iff f = \Theta(g \text{ polylog}(g)).$$

These notations do not remove dominant polylogarithmic factors. For example, if $f = \mathcal{O}(\log g \log \log g)$, then we write $f = \tilde{\mathcal{O}}(\log g)$ rather than $f = \tilde{\mathcal{O}}(1)$.

1. Dyson series expansion of Φ_α

In this section, we introduce the Dyson series expansion of Φ_α in Eq. (1). We use the subindex $\{-1, 1\}$ to relabel the system and bath operator as

$$S_1 = A_S, \quad S_{-1} = A_S^\dagger, \quad B_1 = B_E, \quad B_{-1} = B_E^\dagger.$$

Define the system evolution operator $U_S(t) = \exp(-itH)$. The Dyson series expansion of Φ_α is summarized in the following theorem:

Theorem 5. *Let $\rho_{n+1} = \Phi_\alpha(\rho_n)$, then ρ_{n+1} can be generated by the following three steps:*

$$\begin{aligned} & \bullet \quad \rho_{n+1/3} = U_S(T)\rho_n U_S^\dagger(T) \\ & \bullet \quad \rho_{n+2/3} = \rho_{n+1/3} + \mathbb{E}_{A_S} \left(\sum_n \alpha^{2n} (-1)^n \sum_{k=0}^{2n} (-1)^k \int \frac{g(\omega)}{1+e^{\beta\omega}} G_{2n-k, A_S}^\dagger(\omega) \rho_{n+1/3} G_{k, A_S}(\omega) d\omega \right. \\ & \quad \left. + \sum_n \alpha^{2n} (-1)^n \sum_{k=0}^{2n} (-1)^k \int \frac{g(\omega)e^{\beta\omega}}{1+e^{\beta\omega}} F_{2n-k, A_S}^\dagger(\omega) \rho_{n+1/3} F_{k, A_S}(\omega) d\omega \right); \\ & \bullet \quad \rho_{n+1} = U_S(T)\rho_{n+2/3} U_S^\dagger(T). \end{aligned} \quad (\text{B4})$$

Here

$$\begin{aligned} G_{k, A_S}(\omega) &= \int_{-T < t_1 \leq \dots \leq t_k < T} A_S(t_1) A_S^\dagger(t_2) \cdots S_{(-1)^{k-1}}(t_k) e^{-i\omega \sum_{p=1}^k (-1)^p t_p} f(t_1) \cdots f(t_k) dt_1 \cdots dt_k \\ F_{k, A_S}(\omega) &= \int_{-T < t_1 \leq \dots \leq t_k < T} A_S^\dagger(t_1) A_S(t_2) \cdots S_{(-1)^k}(t_k) e^{i\omega \sum_{p=1}^k (-1)^p t_p} f(t_1) \cdots f(t_k) dt_1 \cdots dt_k. \end{aligned} \quad (\text{B5})$$

Define $\gamma(\omega) = \frac{g(\omega) + g(-\omega)}{1 + \exp(\beta\omega)}$. In the case when A_S is uniformly sampled from a set of coupling operators $\mathcal{A} = \{A^i, -A^i\}_i$ with $\{(A^i)^\dagger\}_i = \{A^i\}_i$, we can rewrite (B4) as

$$\rho_{n+2/3} = \rho_{n+1/3} + \mathbb{E}_{A_S} \left(\sum_n \alpha^{2n} (-1)^n \sum_{k=0}^{2n} (-1)^k \int \gamma(\omega) G_{2n-k, A_S}^\dagger(\omega) \rho_{n+1/3} G_{k, A_S}(\omega) d\omega \right). \quad (\text{B6})$$

Proof. For simplicity, we fixed A_S . We use the subindex $\{-1, 1\}$ to relabel the system and bath operator as

$$S_1 = A_S, S_{-1} = A_S^\dagger, B_1 = B_E, B_{-1} = B_E^\dagger.$$

Recall Eq. (2):

$$H_\alpha(t) = H + H_E + \alpha f(t) \left(A_S \otimes B_E + A_S^\dagger \otimes B_E^\dagger \right), \quad H_E = -\omega Z/2, \quad B_E = |1\rangle\langle 0|.$$

For the dynamics described by

$$\begin{cases} \partial_t \rho(t) = -i[H_\alpha(t), \rho(t)], \\ \rho(-T) = \rho_n \otimes \rho_E, \\ \rho_{n+1} = \mathbb{E}_{H_E, A_S}(\text{Tr}_E \rho(T)), \end{cases} \quad (\text{B7})$$

the evolution operator of the time-dependent Hamiltonian can be expressed using the time-ordered exponential as $U^\alpha(t) := U^\alpha(t; -T) = \mathcal{T} \left(\exp \left(-i \int_{-T}^t H_\alpha(s) ds \right) \right)$, and it satisfies

$$\partial_t U^\alpha(t; -T) = -i H_\alpha(t) U^\alpha(t; -T). \quad (\text{B8})$$

By Duhamel's expression, the Dyson series expansion can be written as $U^\alpha(t; -T) = \sum_{n \geq 0} (-i\alpha)^n U_n(t; -T)$, where

$$U_n(t; -T) = \int_{-T}^t \int_{-T}^{s_1} \cdots \int_{-T}^{s_{n-1}} f(s_1) f(s_2) \cdots f(s_n) U_0(t; s_1) H_{S,B} U_0(s_1; s_2) \cdots H_{S,B} U_0(s_n; -T) ds_n \cdots ds_1. \quad (\text{B9})$$

Here $H_{S,B} = S_1 \otimes B_1 + S_{-1} \otimes B_{-1}$ and $U_0(t; -T) = \exp(-i(t+T)(H + H_E))$. The Heisenberg picture evolution of the bath operator follows $B_{(-1)^p}(t) = e^{(-1)^p i t \omega} B_{(-1)^p}$.

After taking expectation in ω and tracing out the degree of freedom in the environment,

$$\begin{aligned} \Phi_\alpha \rho &= \int g(\omega) \text{Tr}_E[U^\alpha(T)(\rho \otimes \rho_E) U^{\alpha\dagger}(T)](\omega) d\omega \\ &= \sum_{n,m \geq 0} (-i\alpha)^n (i\alpha)^m \int g(\omega) \text{Tr}_E[U_n(T; -T)(\rho \otimes \rho_E) U_m^\dagger(T; -T)](\omega) d\omega \\ &= \sum_{n,m \geq 0} (-1)^n (i\alpha)^{n+m} \int d\omega \int_{-T \leq s_n \leq \cdots \leq s_1 \leq T, -T \leq \tau_m \leq \cdots \leq \tau_1 \leq T} ds_1 \cdots ds_n d\tau_1 \cdots d\tau_m g(\omega) \\ &\quad \sum_{\alpha_i, \beta_j \in \{-1, 1\}} U_S(T) S_{\alpha_1}(s_1) \cdots S_{\alpha_n}(s_n) f(s_1) \cdots f(s_n) U_S(T) \rho U_S^\dagger(T) S_{\beta_m}^\dagger(\tau_m) \cdots S_{\beta_1}^\dagger(\tau_1) U_S^\dagger(T) \\ &\quad f(\tau_1) \cdots f(\tau_m) \text{Tr}_E(B_{\alpha_1}(s_1) \cdots B_{\alpha_n}(s_n) \rho_E B_{\beta_m}^\dagger(\tau_m) \cdots B_{\beta_1}^\dagger(\tau_1)), \end{aligned} \quad (\text{B10})$$

where $U_S(T) = \exp(-iT H)$ and $S_\alpha(t) = \exp(iHt) S_\alpha \exp(-iHt)$. Notice that $B_\alpha^\dagger(t) = B_{-\alpha}(t)$, the multi-point bath correlation function follows

$$\begin{aligned} &\text{Tr}[B_{\alpha_1}(s_1) \cdots B_{\alpha_n}(s_n) \rho_E B_{\beta_m}^\dagger(\tau_m) \cdots B_{\beta_1}^\dagger(\tau_1)] \\ &= \text{Tr}[B_{-\beta_m}(\tau_m) \cdots B_{-\beta_1}(\tau_1) B_{\alpha_1}(s_1) \cdots B_{\alpha_n}(s_n) \rho_E] \\ &= e^{i\phi} \text{Tr}[B_{-\beta_m} \cdots B_{-\beta_1} B_{\alpha_1} \cdots B_{\alpha_n} \rho_E], \end{aligned}$$

where $\phi = \omega \left(\sum_{j=1}^n \alpha_j s_j - \sum_{k=1}^m \beta_k \tau_k \right)$. It can be rewritten as

$$(\cdots) = e^{i\phi} \times \begin{cases} \text{Tr}(|1\rangle\langle 1| \rho_E) = \frac{1}{e^{\beta\omega} + 1}, & \text{if } m+n \text{ even and } (-\beta_m, \dots, -\beta_1, \alpha_1, \dots, \alpha_n) = (1, -1)^{\otimes \frac{m+n}{2}}, \\ \text{Tr}(|0\rangle\langle 0| \rho_E) = \frac{e^{\beta\omega}}{e^{\beta\omega} + 1}, & \text{if } m+n \text{ even and } (-\beta_m, \dots, -\beta_1, \alpha_1, \dots, \alpha_n) = (-1, 1)^{\otimes \frac{m+n}{2}}, \\ 0, & \text{otherwise.} \end{cases} \quad (\text{B11})$$

Substituting the expression of the bath correlation functions back to Eq. (B10), we have

$$\begin{aligned} \Phi_\alpha \rho_n &= U_S(2T) \rho_n U_S(2T)^\dagger \\ &+ \sum_{n \geq 1} \alpha^{2n} (-1)^n \sum_{k=0}^{2n} (-1)^k \int \frac{g(\omega)}{1 + e^{\beta\omega}} U_S(T) G_{2n-k, A_S}^\dagger(\omega) U_S(T) \rho_n U_S^\dagger(T) G_{k, A_S}(\omega) U_S^\dagger(T) d\omega \\ &+ \sum_{n \geq 1} \alpha^{2n} (-1)^n \sum_{k=0}^{2n} (-1)^k \int \frac{g(\omega) e^{\beta\omega}}{1 + e^{\beta\omega}} U_S(T) F_{2n-k, A_S}^\dagger(\omega) U_S(T) \rho_n U_S^\dagger(T) F_{k, A_S}(\omega) U_S^\dagger(T) d\omega, \end{aligned} \quad (\text{B12})$$

where

$$\begin{aligned} G_{k, A_S}(\omega) &= \int_{-T < t_1 \leq \cdots \leq t_k < T} A_S(t_1) A_S^\dagger(t_2) \cdots S_{(-1)^{k-1}}(t_k) e^{-i\omega \sum_{p=1}^k (-1)^p t_p} f(t_1) \cdots f(t_k) dt_1 \cdots dt_k \\ F_{k, A_S}(\omega) &= \int_{-T < t_1 \leq \cdots \leq t_k < T} A_S^\dagger(t_1) A_S(t_2) \cdots S_{(-1)^k}(t_k) e^{i\omega \sum_{p=1}^k (-1)^p t_p} f(t_1) \cdots f(t_k) dt_1 \cdots dt_k. \end{aligned}$$

Additionally, using the relation $F_{k, A_S}^\dagger(-\omega) = G_{k, A_S}(\omega)$, we can further simplify the expression to Eq. (B6) in the case $\mathcal{A}^\dagger = \mathcal{A}$. This concludes the proof. \square

Appendix C: Thermal state preparation beyond Lindblad limit

In this section, we introduce the rigorous version of Theorem 2 and provide the proof. First, recall Theorem 5 (B6),

- $\rho_{n+1/3} = U_S(T)\rho_n U_S^\dagger(T)$;
- $\rho_{n+2/3} = \rho_{n+1/3} + \mathbb{E}_{A_S} \left(\sum_n \alpha^{2n} (-1)^n \sum_{k=0}^{2n} (-1)^k \int \gamma(\omega) G_{2n-k, A_S}^\dagger(\omega) \rho_{n+1/3} G_{k, A_S}(\omega) d\omega \right)$;
- $\rho_{n+1} = U_S(T)\rho_{n+2/3} U_S^\dagger(T)$.

We present the rigorous version of Theorem 2 in the following:

Theorem 6 (Thermal state, rigorous version). *Assume $0 \leq \beta < \infty$ and $\gamma(\omega)$ satisfies the property:*

- *decay fast at infinity, i.e. $\lim_{|\omega| \rightarrow \infty} \gamma(\omega) = 0$.*
- $\gamma'(\omega), (\tilde{\gamma}(\omega))' \in L^1$.

where $\tilde{\gamma}(\omega) = \gamma(\omega)e^{\beta\omega}$. Assume $\alpha = \mathcal{O}(\sigma^{-1/2})$, $\sigma = \Omega(\beta)$, and $T = \Omega(\sigma)$. Then,

$$\|\Phi_\alpha \sigma_\beta - \sigma_\beta\|_1 < \mathcal{O} \left(\frac{\beta \alpha^2}{\sigma} ((\|\gamma'\|_{L^1} + \|\tilde{\gamma}'\|_{L^1}) \log(\sigma)) + \frac{\alpha^2 \sigma^2}{T} e^{-T^2/(4\sigma^2)} \right). \quad (\text{C1})$$

Furthermore, if Φ_α has mixing time $\tau_{\text{mix}, \Phi_\alpha}$, we have

$$\|\rho_{\text{fix}}(\Phi_\alpha) - \sigma_\beta\|_1 = \mathcal{O} \left(\tau_{\text{mix}, \Phi_\alpha} \left(\frac{\beta \alpha^2}{\sigma} ((\|\gamma'\|_{L^1} + \|\tilde{\gamma}'\|_{L^1}) \log(\sigma)) + \frac{\alpha^2 \sigma^2}{T} e^{-T^2/(4\sigma^2)} \right) \right).$$

Now, we provide the proof of Theorem 6. Letting $T \rightarrow \infty$, we define

$$\tilde{G}_{k, A_S}(\omega) := \int_{-\infty < t_1 \leq \dots \leq t_k < \infty} A_S(t_1) A_S^\dagger(t_2) \dots e^{-i\omega \sum_{p=1}^k (-1)^p t_p} f(t_1) \dots f(t_k) dt_1 \dots dt_k, \quad (\text{C2})$$

and the limiting CPTP map

$$\tilde{\Phi}_\alpha := U_S(2T)\rho_n U_S^\dagger(2T) + \mathbb{E}_{A_S} \left(\sum_{n \geq 1} \alpha^{2n} (-1)^n \sum_{k=0}^{2n} (-1)^k \int \gamma(\omega) U_S(T) \tilde{G}_{2n-k, A_S}^\dagger(\omega) U_S(T) \rho_n U_S^\dagger(T) \tilde{G}_{k, A_S}(\omega) U_S^\dagger(T) d\omega \right). \quad (\text{C3})$$

The distance between Φ_α and $\tilde{\Phi}_\alpha$ can be controlled in the following lemma:

Lemma 7. *When $\alpha = \mathcal{O}(\sigma^{-1/2})$, we have*

$$\|\Phi_\alpha - \tilde{\Phi}_\alpha\|_{1 \rightarrow 1} = \mathcal{O} \left(\frac{\alpha^2 \sigma^2}{T} e^{-T^2/(4\sigma^2)} \right). \quad (\text{C4})$$

Proof of Lemma 7. For simplicity, we only consider the case when $\mathcal{A} = \{A_S, -A_S\}$ is fixed. The general case is almost the same. By the general expression of the dynamic map, we have

$$\begin{aligned} & \|\Phi_\alpha - \tilde{\Phi}_\alpha\|_{1 \rightarrow 1} \\ & \leq \max_{\rho_n: \|\rho_n\|=1} \sum_{n \geq 1} \alpha^{2n} \sum_{k=0}^{2n} \int |\gamma(\omega)| \left\| \tilde{G}_{2n-k, A_S}^\dagger(\omega) U_S(T) \rho_n U_S^\dagger(T) \tilde{G}_{k, A_S}(\omega) - G_{2n-k, A_S}^\dagger(\omega) U_S(T) \rho_n U_S^\dagger(T) G_{k, A_S}(\omega) \right\|_1 d\omega \\ & \leq \sum_{n \geq 1} \alpha^{2n} \sum_{k=0}^{2n} \int |\gamma(\omega)| \left\| \tilde{G}_{2n-k, A_S}^\dagger(\omega) - G_{2n-k, A_S}^\dagger(\omega) \right\| \left\| \tilde{G}_{k, A_S}(\omega) \right\| d\omega \\ & \quad + \sum_{n \geq 1} \alpha^{2n} \sum_{k=0}^{2n} \int |\gamma(\omega)| \left\| G_{2n-k, A_S}^\dagger(\omega) \right\| \left\| G_{k, A_S}(\omega) - \tilde{G}_{k, A_S}(\omega) \right\| d\omega \end{aligned} \quad (\text{C5})$$

It is sufficient to bound $\|G_{k,A_S}(\omega) - \tilde{G}_{k,A_S}(\omega)\|$ and $\|G_{k,A_S}(\omega)\|$, $\|\tilde{G}_{k,A_S}(\omega)\|$. For the first term, we have

$$\begin{aligned}
& \|G_{k,A_S}(\omega) - \tilde{G}_{k,A_S}(\omega)\| \\
& \leq \left\| \left(\int_{-\infty < t_1 \leq \dots \leq t_k < \infty} - \int_{-T < t_1 \leq \dots \leq t_k < T} \right) A_S(t_1) A_S^\dagger(t_2) \dots e^{-i\omega \sum_{p=1}^k (-1)^p t_p} f(t_1) \dots f(t_k) dt_1 \dots dt_k \right\| \\
& \leq \left\| \int_{t_1 \leq \dots \leq t_k, \max_i |t_i| \geq T} A_S(t_1) A_S^\dagger(t_2) \dots e^{-i\omega \sum_{p=1}^k (-1)^p t_p} f(t_1) \dots f(t_k) dt_1 \dots dt_k \right\| \\
& \leq \|A_S\|^k \int_{t_1 \leq \dots \leq t_k} \chi_{\max_i |t_i| \geq T} f(t_1) \dots f(t_k) dt_1 \dots dt_k = \frac{\|A_S\|^k}{(k-1)!} \left(\int_{\mathbb{R}} f(t) dt \right)^{k-1} \int_{|t| \geq T} f(t) dt \\
& = \frac{(\mathcal{O}(\sigma^{1/2}))^k}{(k-1)!} \frac{\sigma}{T} e^{-T^2/(4\sigma^2)}
\end{aligned} \tag{C6}$$

where we use $\|A_S\| \leq 1$ in the last inequality.

For the second term, we have

$$\|G_{k,A_S}(\omega)\| \leq \|\tilde{G}_{k,A_S}(\omega)\| \leq \|A_S\|^k \int_{-\infty < t_1 \leq \dots \leq t_k < \infty} |f(t_1)| \dots |f(t_k)| dt_1 \dots dt_k = \frac{(\mathcal{O}(\sigma^{1/2}))^k}{k!} \tag{C7}$$

Combining these two bounds and $\|\gamma\|_{L^1} = 1$, we have

$$\begin{aligned}
\|\Phi_\alpha - \tilde{\Phi}_\alpha\|_{1 \rightarrow 1} & \leq \frac{\sigma}{T} e^{-T^2/(4\sigma^2)} \sum_{n \geq 1} \alpha^{2n} \sum_{k=0}^{2n} \left(\frac{(\mathcal{O}(\sigma^{1/2}))^{2n}}{(2n-k-1)!k!} + \frac{(\mathcal{O}(\sigma^{1/2}))^{2n}}{(2n-k)!(k-1)!} \right) \\
& = \mathcal{O} \left(\frac{\alpha^2 \sigma^2}{T} e^{-T^2/(4\sigma^2)} \sum_{n \geq 1} \frac{1}{(2n-2)!} (\mathcal{O}(\alpha \sigma^{1/2}))^{2n-2} \right) = \mathcal{O} \left(\frac{\alpha^2 \sigma^2}{T} e^{-T^2/(4\sigma^2)} \right).
\end{aligned} \tag{C8}$$

□

Using $\tilde{\Phi}_\alpha$, we have

$$\|\Phi_\alpha \sigma_\beta - \sigma_\beta\|_1 \leq \|\tilde{\Phi}_\alpha \sigma_\beta - \Phi_\alpha \sigma_\beta\|_1 + \|\tilde{\Phi}_\alpha \sigma_\beta - \sigma_\beta\|_1 \leq \|\tilde{\Phi}_\alpha - \Phi_\alpha\|_{1 \rightarrow 1} + \|\tilde{\Phi}_\alpha \sigma_\beta - \sigma_\beta\|_1. \tag{C9}$$

Thus, it suffices to show $\|\tilde{\Phi}_\alpha \sigma_\beta - \sigma_\beta\|_1$ is small. Instead of relying directly on the detailed-balance condition of the Lindblad equation, we make use of an intrinsic property of the channel, namely $\tilde{\Phi}_\alpha^\dagger I = I$. This condition is significantly easier to incorporate into the arbitrary-order expansion.

Lemma 8. (Avoid Detailed Balance Condition) *We have*

$$\mathbb{E}_{A_S} \left(\sum_n \alpha^{2n} (-1)^n \sum_{k=0}^{2n} (-1)^k \int \gamma((-1)^k \omega) \tilde{G}_{2n-k, A_S}^\dagger(\omega) \tilde{G}_{k, A_S}(\omega) d\omega \right) = 0. \tag{C10}$$

Proof. See Appendix C1. □

In order to prove $\tilde{\Phi}_\alpha$ preserves the thermal state, with Lemma 8, it suffices to bound the following terms for each

A_S :

$$\begin{aligned}
& \left\| \sum_{n \geq 1} \alpha^{2n} (-1)^n \sum_{k=0}^{2n} (-1)^k \int \gamma(\omega) \tilde{G}_{2n-k, A_S}^\dagger(\omega) \sigma_\beta \tilde{G}_{k, A_S}(\omega) d\omega \right\|_1 \\
& \leq \underbrace{\left\| \sum_{n \geq 1} \alpha^{2n} (-1)^n \left(\sum_{k=0, \text{even}}^{2n} (-1)^k \int \gamma(\omega) \tilde{G}_{2n-k, A_S}^\dagger(\omega) \sigma_\beta \tilde{G}_{k, A_S}(\omega) d\omega - \sigma_\beta \int \gamma(\omega) \tilde{G}_{2n-k, A_S}^\dagger(\omega) \tilde{G}_{k, A_S}(\omega) d\omega \right) \right\|_1}_{\text{Term 1}} \\
& + \underbrace{\left\| \sum_{n \geq 1} \alpha^{2n} (-1)^n \left(\sum_{k=0, \text{odd}}^{2n} (-1)^k \int \gamma(\omega) \tilde{G}_{2n-k, A_S}^\dagger(\omega) \sigma_\beta \tilde{G}_{k, A_S}(\omega) d\omega - \sigma_\beta \int \underbrace{\gamma(\omega) \exp(\beta\omega)}_{=\gamma(-\omega)} \tilde{G}_{2n-k, A_S}^\dagger(\omega) \tilde{G}_{k, A_S}(\omega) d\omega \right) \right\|_1}_{\text{Term 2}} \tag{C11}
\end{aligned}$$

The analysis of both Term 1 and Term 2 can be simplified to the bound for $\sigma_\beta^{-1} \tilde{G}_{2n-k, A_S}^\dagger(\omega) \sigma_\beta - \tilde{G}_{2n-k, A_S}^\dagger$. For example, Term 1 can be rewritten as

$$\text{Term 1} = \left\| \sigma_\beta \sum_{n \geq 1} \alpha^{2n} (-1)^n \left(\sum_{k=0, \text{even}}^{2n} (-1)^k \int \gamma(\omega) \left(\sigma_\beta^{-1} \tilde{G}_{2n-k, A_S}^\dagger(\omega) \sigma_\beta - \tilde{G}_{2n-k, A_S}^\dagger \right) \tilde{G}_{k, A_S}(\omega) d\omega \right) \right\|_1 \tag{C12}$$

In order to analyze this term, we introduce the following lemma to obtain an explicit expression for this difference.

Lemma 9. *We have*

$$\begin{aligned}
& \sigma_\beta^{-1} \tilde{G}_{k, A_S}^\dagger(\omega) \sigma_\beta = \frac{(2\sigma^{1/2})^k}{((2\pi)^{1/4})^k} \int_{-\infty < \tau_1 \leq \dots \leq \tau_k < \infty} \dots A_S(2\sigma\tau_2) A_S^\dagger(2\sigma\tau_1) \\
& \exp \left(i2\sigma\omega \sum_{p=1}^k (-1)^p \tau_p - \omega\beta\Lambda(k) - \sum_{p=1}^k \tau_p^2 + \frac{k\beta^2}{4\sigma^2} - i\frac{\beta}{\sigma} \sum_{p=1}^k \tau_p \right) d\tau_1 \dots d\tau_k. \tag{C13}
\end{aligned}$$

$$\text{where } \Lambda(k) = \begin{cases} 0 & \text{When } k \text{ is even} \\ -1 & \text{When } k \text{ is odd} \end{cases}.$$

Proof. See Appendix C2. \square

In the following part of the proof, we assume that A_S is Hermitian to simplify the notation. The calculation for non-hermitian A_S is the same. By substituting Eq. (C13) to Term 1, we have

$$\begin{aligned}
\text{Term 1} & \leq \|\sigma_\beta\|_1 \sum_{n \geq 1} \frac{(2\alpha\sigma^{1/2})^{2n}}{((2\pi)^{1/4})^{2n}} \sum_{\substack{k=0 \\ \text{even}}}^{2n} \left\| \int_{-\infty < s_1 \leq s_2 \leq \dots \leq s_{2n-k} < \infty, -\infty < t_1 \leq t_2 \leq \dots \leq t_k < \infty} A_S(2\sigma s_{2n-k}) \dots A_S(2\sigma s_1) \right. \\
& \quad \left. A_S(2\sigma t_1) \dots A_S(2\sigma t_k) e^{-\sum_{p=1}^{2n-k} s_p^2 - \sum_{p=1}^k t_p^2} \right. \\
& \quad \left. \int \gamma(\omega) e^{i2\sigma\omega \sum_{p=1}^{2n-k} (-1)^p s_p - i2\sigma\omega \sum_{p=1}^k (-1)^p t_p} d\omega \left(\exp \left(\frac{(2n-k)\beta^2}{4\sigma^2} - i\frac{\beta}{\sigma} \sum_{p=1}^{2n-k} s_p \right) - 1 \right) ds_1 \dots ds_{2n-k} dt_1 \dots dt_k \right\| \\
& \leq \sum_{n \geq 1} \frac{(2\alpha\sigma^{1/2})^{2n}}{((2\pi)^{1/4})^{2n}} \|A_S\|^{2n} \sum_{\substack{k=0 \\ \text{even}}}^{2n} \int_{-\infty < s_1 \leq s_2 \leq \dots \leq s_{2n-k} < \infty, -\infty < t_1 \leq t_2 \leq \dots \leq t_k < \infty} e^{-\sum_{p=1}^{2n-k} s_p^2 - \sum_{p=1}^k t_p^2} \\
& \quad \left| \int \gamma(\omega) e^{i2\sigma\omega \sum_{p=1}^{2n-k} (-1)^p s_p - \sum_{p=1}^k (-1)^p t_p} d\omega \right| \left| \exp \left(\frac{(2n-k)\beta^2}{4\sigma^2} - i\frac{\beta}{\sigma} \sum_{p=1}^{2n-k} s_p \right) - 1 \right| ds_1 \dots ds_{2n-k} dt_1 \dots dt_k. \tag{C14}
\end{aligned}$$

It is sufficient to show the following term is upper bounded by $C_{n,k} \frac{\beta}{\sigma^2}$, with the preconstant $C_{n,k}$ depend on n and k ,

$$\begin{aligned}
& \int_{-\infty < s_1 \leq s_2 \leq \dots \leq s_{2n-k} < \infty, -\infty < t_1 \leq t_2 \leq \dots \leq t_k < \infty} e^{-\sum_{p=1}^{2n-k} s_p^2 - \sum_{p=1}^k t_p^2} \\
& \left| \int \gamma(\omega) e^{i2\sigma\omega(\sum_{p=1}^{2n-k} (-1)^p s_p - \sum_{p=1}^k (-1)^p t_p)} d\omega \right| \left| \exp \left(\frac{(2n-k)\beta^2}{4\sigma^2} - i\frac{\beta}{\sigma} \sum_{p=1}^{2n-k} s_p \right) - 1 \right| ds_1 \dots ds_{2n-k} dt_1 \dots dt_k \\
& \leq \int_{-\infty < s_1 \leq s_2 \leq \dots \leq s_{2n-k} < \infty, -\infty < t_1 \leq t_2 \leq \dots \leq t_k < \infty} e^{-\sum_{p=1}^{2n-k} s_p^2 - \sum_{p=1}^k t_p^2} \\
& \underbrace{\left| \int \gamma(\omega) e^{i2\sigma\omega(\sum_{p=1}^{2n-k} (-1)^p s_p - \sum_{p=1}^k (-1)^p t_p)} d\omega \right| \exp \left(\frac{(2n-k)\beta^2}{4\sigma^2} \right) \left| \exp \left(-i\frac{\beta}{\sigma} \sum_{p=1}^{2n-k} s_p \right) - 1 \right| ds_1 \dots ds_{2n-k} dt_1 \dots dt_k}_{\text{Term 1.1}} \\
& + \int_{-\infty < s_1 \leq s_2 \leq \dots \leq s_{2n-k} < \infty, -\infty < t_1 \leq t_2 \leq \dots \leq t_k < \infty} e^{-\sum_{p=1}^{2n-k} s_p^2 - \sum_{p=1}^k t_p^2} \\
& \underbrace{\left| \int \gamma(\omega) e^{i2\sigma\omega(\sum_{p=1}^{2n-k} (-1)^p s_p - \sum_{p=1}^k (-1)^p t_p)} d\omega \right| \left| \exp \left(\frac{(2n-k)\beta^2}{4\sigma^2} \right) - 1 \right| ds_1 \dots ds_{2n-k} dt_1 \dots dt_k}_{\text{Term 1.2}}. \tag{C15}
\end{aligned}$$

We bound Term 1.1 and Term 1.2 separately, with detailed calculation in Appendix C 3,

- For Term 1.1,

$$\text{Term 1.1} = \frac{\beta(2\pi)^n}{\sigma^2} \exp \left(\frac{(2n-k)\beta^2}{4\sigma^2} \right) \mathcal{O} \left(\|\gamma'\|_{L^1} \log(\sqrt{2n}\sigma) + \frac{1}{n} \right). \tag{C16}$$

- For Term 1.2,

$$\text{Term 1.2} = \frac{(2\pi)^n}{\sigma\sqrt{n}} \left| \exp \left(\frac{(2n-k)\beta^2}{4\sigma^2} \right) - 1 \right| \mathcal{O} \left(\|\gamma'\|_{L^1} \log(\sqrt{2n}\sigma) + \frac{\sqrt{n}}{\sigma} \right). \tag{C17}$$

Then

$$\begin{aligned}
\text{Term 1} & \leq \sum_{n \geq 1} \frac{\alpha^{2n} \sigma^n}{\sqrt{2\pi}^n} \sum_{k=0}^{2n} \left(\frac{\beta(2\pi)^n}{\sigma^2} \exp \left(\frac{(2n-k)\beta^2}{4\sigma^2} \right) \mathcal{O} \left(\|\gamma'\|_{L^1} \log(\sqrt{2n}\sigma) + \frac{1}{n} \right) \right. \\
& \quad \left. + \frac{(2\pi)^n}{\sqrt{n}\sigma} \left| \exp \left(\frac{(2n-k)\beta^2}{4\sigma^2} \right) - 1 \right| \mathcal{O} \left(\log(\sqrt{2n}\sigma) \|\gamma'\|_{L^1} + \frac{\sqrt{n}}{\sigma} \right) \right). \tag{C18}
\end{aligned}$$

With $r = r(\sigma, \beta) := \exp(\beta^2/(2\sigma^2)) > 1$ and $R = R(\sigma, \alpha) := \pi^{1/2} \sigma \alpha^2 r$, we have

$$\begin{aligned}
\text{Term 1} & \leq \mathcal{O} \left(\frac{\beta \|\gamma'\|_{L^1}}{\sigma^2} \sum_{n \geq 1} (n+1) \log(\sqrt{2n}\sigma) R^n + \frac{\beta}{\sigma^2} \sum_{n \geq 1} \frac{n+1}{n} R^n \right. \\
& \quad \left. + \frac{\|\gamma'\|_{L^1}}{\sigma} \sum_{n \geq 1} \frac{n+1}{\sqrt{n}} \log(\sqrt{2n}\sigma) \left(R^n - \frac{R^n}{r^n} \right) + \frac{1}{\sigma^2} \sum_{n \geq 1} (n+1) \left(R^n - \frac{R^n}{r^n} \right) \right). \tag{C19}
\end{aligned}$$

Let $\theta = \beta^2/\sigma^2$. With the bound of the polylogarithm function and $r-1 = \mathcal{O}(\theta)$, we have

$$\text{Term 1} \leq \frac{\beta R \|\gamma'\|_{L^1}}{\sigma^2} \mathcal{O}(1 + \log(\sigma)) + \frac{\beta R}{\sigma^2} \mathcal{O}(1) + \frac{\|\gamma'\|_{L^1} R \theta}{\sigma} \mathcal{O}(1 + \log(\sigma)) + \frac{R \theta}{\sigma^2} \mathcal{O}(1) \tag{C20}$$

when $R < 1$ and $\theta R < 1$ (i.e., $\sigma \alpha^2 = \mathcal{O}(1)$ and $\alpha^2/\sigma = \mathcal{O}(1)$). Substitute the expression of R, r, θ back to the bound, we have

$$\text{Term 1} \leq \frac{\beta \alpha^2}{\sigma} \exp(\beta^2/\sigma^2) \mathcal{O} \left(\|\gamma'\|_{L^1} \left(\log(\sigma) + 1 \right) \left(1 + \frac{\beta}{\sigma} \right) \right) = \mathcal{O} \left(\frac{\beta \alpha^2 \log(\sigma)}{\sigma} \|\gamma'\|_{L^1} \right). \tag{C21}$$

when

$$\pi^{1/2}\sigma\alpha^2 \exp(\beta^2/(2\sigma^2)) < 1, \quad \frac{\pi^{1/2}\beta^2\alpha^2}{\sigma} \exp(\beta^2/(2\sigma^2)) < 1. \quad (\text{C22})$$

When k is odd, the bound for Term 2 is obtained in exactly the same way, with $\gamma(\omega)$ replaced by $\tilde{\gamma}(\omega) = \gamma(\omega)\exp(\beta\omega)$. In particular, the additional factor $e^{\beta\omega}$ in $\tilde{\gamma}(\omega)$ is precisely the one appearing in Eq. (C13) for odd indices. Similar to Eq. (C14) and Eq. (C21), we have

$$\begin{aligned} \text{Term 2} &\leq \sum_{n \geq 1} \frac{(2\alpha\sigma^{1/2})^{2n}}{((2\pi)^{1/4})^{2n}} \|A_S\|^{2n} \sum_{\substack{k=0 \\ \text{odd}}}^{2n} \int_{-\infty < s_1 \leq s_2 \leq \dots \leq s_{2n-k} < \infty, -\infty < t_1 \leq t_2 \leq \dots \leq t_k < \infty} e^{-\sum_{p=1}^{2n-k} s_p^2 - \sum_{p=1}^k t_p^2} \\ &\quad \left| \int \tilde{\gamma}(\omega) e^{i2\sigma\omega(\sum_{p=1}^{2n-k} (-1)^p s_p - \sum_{p=1}^k (-1)^p t_p)} d\omega \right| \left| \exp \left(\frac{(2n-k)\beta^2}{4\sigma^2} - i\frac{\beta}{\sigma} \sum_{p=1}^{2n-k} s_p \right) - 1 \right| ds_1 \dots ds_{2n-k} dt_1 \dots dt_k \\ &= \mathcal{O} \left(\frac{\beta\alpha^2 \log(\sigma)}{\sigma} \|\tilde{\gamma}'\|_{L_1} \right). \end{aligned} \quad (\text{C23})$$

Summing all terms, we conclude the proof of Theorem 6.

1. Proof of Lemma 8

Notice that the expression of $\tilde{G}_{k,A_S}(\omega)$ depends on the system Hamiltonian H and the coupling operator A_S . We define

$$\tilde{G}_{k,H,A_S}(\omega) = \tilde{G}_{k,A_S}(\omega) = \int_{-\infty < t_1 \leq \dots \leq t_k < \infty} A_S(t_1) A_S^\dagger(t_2) \dots e^{-i\omega \sum_{p=1}^k (-1)^p t_p} f(t_1) \dots f(t_k) dt_1 \dots dt_k.$$

Then,

$$\begin{aligned} \tilde{G}_{k,H,A_S}^\dagger(\omega) &= \int_{-\infty < t_1 \leq \dots \leq t_k < \infty} \dots A_S(t_2) A_S^\dagger(t_1) e^{i\omega \sum_{p=1}^k (-1)^p t_p} f(t_1) \dots f(t_k) dt_1 \dots dt_k \\ &= \int_{-\infty < s_1 \leq \dots \leq s_k < \infty} \dots A_S(-s_{k-1}) A_S^\dagger(-s_k) e^{-i\omega(-1)^{k-1} \sum_{p=1}^k (-1)^p s_p} f(s_1) \dots f(s_k) dt_1 \dots dt_k, \quad s_j = -t_{k-j+1} \\ &= \begin{cases} \tilde{G}_{k,-H,A_S^\dagger}(\omega), & k \text{ odd}, \\ \tilde{G}_{k,-H,A_S}(-\omega), & k \text{ even}. \end{cases} \end{aligned}$$

Similarly, we have

$$\tilde{G}_{k,H,A_S}(\omega) = \begin{cases} \tilde{G}_{k,-H,A_S^\dagger}^\dagger(\omega), & k \text{ odd} \\ \tilde{G}_{k,-H,A_S}^\dagger(-\omega), & k \text{ even} \end{cases}.$$

Now, we generate evolution operator $\tilde{\Psi}_\alpha$, defined in analogy with $\tilde{\Phi}_\alpha$, by replacing Hamiltonian in \tilde{G}_k with $-H$ and inverse temperature with $-\beta$,

$$\begin{aligned} \tilde{\Psi}_\alpha \rho_0 &= \int g(\omega) \text{Tr}_E[U^\alpha(T)(\rho_0 \otimes \rho_E)U^{\alpha\dagger}(T)](\omega) d\omega \\ &= U_S(2T)\rho_0 U_S^\dagger(2T) \\ &\quad + \mathbb{E}_{A_S} \left(\sum_n \alpha^{2n} (-1)^n \sum_{k=0}^{2n} (-1)^k \int \underbrace{\frac{g(\omega) + g(-\omega)}{1 + e^{-\beta\omega}}}_{=\gamma(-\omega)} U_S(T) \tilde{G}_{2n-k,-H,A_S}^\dagger(\omega) U_S(T) \rho_0 U_S^\dagger(T) \tilde{G}_{k,-H,A_S}(\omega) U_S^\dagger(T) d\omega \right) \end{aligned}$$

It is straightforward to see that $\tilde{\Psi}_\alpha$ is a quantum channel. This implies

$$\tilde{\Psi}_\alpha^\dagger[I] = I \Rightarrow \mathbb{E}_{A_S} \left(\sum_n \alpha^{2n} (-1)^n \sum_{k=0}^{2n} (-1)^k \int \gamma(-\omega) \tilde{G}_{2n-k,-H,A_S}(\omega) \tilde{G}_{k,-H,A_S}^\dagger(\omega) d\omega \right) = 0.$$

Because $\{(A_i)^\dagger\} = \{A_i\}$, we have

$$\begin{aligned}
& \mathbb{E}_{A_S} \left(\sum_n \alpha^{2n} (-1)^n \sum_{k=0}^{2n} (-1)^k \int \gamma((-1)^k \omega) \tilde{G}_{2n-k, H, A_S}^\dagger(\omega) \tilde{G}_{k, H, A_S}(\omega) d\omega \right) \\
&= \mathbb{E}_{A_S} \left(\sum_n \alpha^{2n} (-1)^n \sum_{k=0, \text{even}}^{2n} (-1)^k \int \gamma(\omega) \tilde{G}_{2n-k, -H, A_S}(-\omega) \tilde{G}_{k, -H, A_S}^\dagger(-\omega) d\omega \right) \\
&+ \underbrace{\mathbb{E}_{A_S} \left(\sum_n \alpha^{2n} (-1)^n \sum_{k=0, \text{odd}}^{2n} (-1)^k \int \gamma(-\omega) \tilde{G}_{2n-k, -H, A_S}^\dagger(\omega) \tilde{G}_{k, -H, A_S}^\dagger(\omega) d\omega \right)}_{= \mathbb{E}_{A_S} \left(\sum_n \alpha^{2n} (-1)^n \sum_{k=0, \text{odd}}^{2n} (-1)^k \int \gamma(-\omega) \tilde{G}_{2n-k, -H, A_S}(\omega) \tilde{G}_{k, -H, A_S}^\dagger(\omega) d\omega \right)} \\
&= \mathbb{E}_{A_S} \left(\sum_n \alpha^{2n} (-1)^n \sum_{k=0}^{2n} (-1)^k \int \gamma(-\omega) \tilde{G}_{2n-k, -H, A_S}(\omega) \tilde{G}_{k, -H, A_S}^\dagger(\omega) d\omega \right) = 0,
\end{aligned} \tag{C24}$$

The proof is complete.

2. Proof of Lemma 9

The main goal of this section is to prove an explicit expression of $\sigma_\beta^{-1} \tilde{G}_{k, A_S}^\dagger \sigma_\beta$. We show that it admits the same structural form as $\tilde{G}_{k, A_S}^\dagger$ after a β -dependent shift of the integration variable. In addition, for notation simplicity, we assume A_S is hermitian. The extension to the non-hermitian A_S is straightforward.

We first calculate $\sigma_\beta^{-1} \tilde{G}_{k, A_S} \sigma_\beta$, the expression of $\sigma_\beta^{-1} \tilde{G}_{k, A_S}^\dagger \sigma_\beta$ can be obtained by applying the complex conjugate on it. We apply the change of variable,

$$t_p = \sum_{q=p}^k s_q, \forall p = 1, \dots, k \Leftrightarrow \begin{cases} s_p = t_p - t_{p+1}, & 1 \leq p < k \\ s_k = t_k & \end{cases}. \tag{C25}$$

to \tilde{G}_{k, A_S} in Eq. (C2), then

$$\tilde{G}_{k, A_S}(\omega) = \int_{-\infty < s_1, \dots, s_{k-1} \leq 0, -\infty < s_k < \infty} A_S \left(\sum_{p=1}^k s_p \right) \dots A_S(s_k) e^{-i\omega \sum_{p=1}^k (-1)^p \sum_{q=p}^k s_q} f \left(\sum_{p=1}^k s_p \right) \dots f(s_k) ds_1 \dots ds_k. \tag{C26}$$

Notice that applying the commutator once on the product of system operators is equivalent to differentiating with respect to s_k ,

$$\left[H, A_S \left(\sum_{p=1}^k s_p \right) \dots A_S(s_k) \right] = -i\partial_{s_k} \left(A_S \left(\sum_{p=1}^k s_p \right) \dots A_S(s_k) \right). \tag{C27}$$

By integration by parts, we have

$$\begin{aligned}
\left[H, \tilde{G}_{k, A_S} \right] &= \int_{-\infty < s_1, \dots, s_{k-1} \leq 0, -\infty < s_k < \infty} A_S \left(\sum_{p=1}^k s_p \right) \dots A_S(s_k) \\
&\quad i\partial_{s_k} \left(e^{-i\omega \sum_{p=1}^k (-1)^p \sum_{q=p}^k s_q} f \left(\sum_{p=1}^k s_p \right) \dots f(s_k) \right) ds_1 \dots ds_k.
\end{aligned} \tag{C28}$$

It reveals that when we apply the commutator operator m times,

$$\begin{aligned}
& \underbrace{\left[H, \left[H, \dots, \left[H, \tilde{G}_{k, A_S} \right] \right] \right]}_{m \text{ commutator}} = \int_{-\infty < s_1, \dots, s_{k-1} \leq 0, -\infty < s_k < \infty} A_S \left(\sum_{p=1}^k s_p \right) \dots A_S(s_k) \\
& i^m \partial_{s_k}^m \left(e^{-i\omega \sum_{p=1}^k (-1)^p \sum_{q=p}^k s_q} f \left(\sum_{p=1}^k s_p \right) \dots f(s_k) \right) ds_1 \dots ds_k.
\end{aligned} \tag{C29}$$

We use the Baker–Campbell–Hausdorff formula to expand $\sigma_\beta \tilde{G}_{k,A_S} \sigma_\beta^{-1}$ as a series of the commutators,

$$\begin{aligned}
\sigma_\beta \tilde{G}_{k,A_S} \sigma_\beta^{-1} &= \tilde{G}_{k,A_S} + (-\beta) \left[H, \tilde{G}_{k,A_S} \right] + \frac{1}{2!} (-\beta)^2 \left[H, \left[H, \tilde{G}_{k,A_S} \right] \right] + \cdots + \frac{1}{m!} (-\beta)^m \underbrace{\left[H, \left[H, \cdots, \left[H, \tilde{G}_{k,A_S} \right] \right] \right]}_{m \text{ commutator}} + \cdots \\
&= \int_{-\infty < s_1, \dots, s_{k-1} \leq 0, -\infty < s_k < \infty} A_S \left(\sum_{p=1}^k s_p \right) \cdots A_S(s_k) \\
&\quad \sum_{n \geq 0} \frac{1}{m!} (-\beta)^m i^m \partial_{s_k}^m \left(e^{-i\omega \sum_{p=1}^k (-1)^p \sum_{q=p}^k s_q} f \left(\sum_{p=1}^k s_p \right) \cdots f(s_k) \right) ds_1 \cdots ds_k \\
&= \int_{-\infty < s_1, \dots, s_{k-1} \leq 0, -\infty < s_k < \infty} A_S \left(\sum_{p=1}^k s_p \right) \cdots A_S(s_k) \\
&\quad \left(e^{-i\omega \sum_{p=1}^{k-1} (-1)^p \sum_{q=p}^{k-1} s_q - i\omega(s_k - i\beta) \sum_{p=1}^k (-1)^p} f(s_1 + \cdots + s_k - i\beta) \cdots f(s_k - i\beta) \right) ds_1 \cdots ds_k. \tag{C30}
\end{aligned}$$

where the last equality follows from Taylor expansion in s_k . Substituting the expression of $f(t)$ yields,

$$\begin{aligned}
\sigma_\beta \tilde{G}_{k,A_S} \sigma_\beta^{-1} &= \int_{-\infty < s_1, \dots, s_{k-1} \leq 0, -\infty < s_k < \infty} A_S \left(\sum_{p=1}^k s_p \right) \cdots A_S(s_k) e^{-i\omega \sum_{p=1}^k (-1)^p \sum_{q=p}^k s_q - \omega\beta \sum_{p=1}^k (-1)^p} \\
&\quad \exp \left(-\frac{1}{4\sigma^2} \sum_{p=1}^k \left(\sum_{q=p}^k s_q - i\beta \right)^2 \right) \left(\frac{1}{(2\pi)^{1/4} \sigma^{1/2}} \right)^k ds_1 \cdots ds_k \tag{C31}
\end{aligned}$$

By rescaling the variable $s_q \rightarrow 2\sigma s_q$ for $q = 1, \dots, k$, we have

$$\begin{aligned}
\sigma_\beta \tilde{G}_{k,A_S} \sigma_\beta^{-1} &= \frac{(2\sigma)^k}{((2\pi)^{1/4} \sigma^{1/2})^k} \int_{-\infty < s_1, \dots, s_{k-1} \leq 0, -\infty < s_k < \infty} A_S \left(2\sigma \sum_{p=1}^k s_p \right) \cdots A_S(2\sigma s_k) \\
&\quad e^{-i2\sigma\omega \sum_{p=1}^k (-1)^p \sum_{q=p}^k s_q - \omega\beta \sum_{p=1}^k (-1)^p} \exp \left(-\sum_{p=1}^k \left(\sum_{q=p}^k s_q \right)^2 \right) \exp \left(\frac{k\beta^2}{4\sigma^2} + i\frac{\beta}{\sigma} (s_1 + 2s_2 + \cdots + ks_k) \right) ds_1 \cdots ds_k. \tag{C32}
\end{aligned}$$

Define the function

$$\Lambda(k) := \sum_{p=1}^k (-1)^p = \begin{cases} 0 & \text{When } k \text{ is even} \\ -1 & \text{When } k \text{ is odd} \end{cases}, \tag{C33}$$

and apply the conjugate transpose to Eq. (C32), we have

$$\begin{aligned}
\sigma_\beta^{-1} \tilde{G}_{k,A_S}^\dagger \sigma_\beta &= \frac{(2\sigma^{1/2})^k}{((2\pi)^{1/4})^k} \int_{-\infty < s_1, \dots, s_{k-1} \leq 0, -\infty < s_k < \infty} A_S(2\sigma s_k) \cdots A_S \left(2\sigma \sum_{p=1}^k s_p \right) \\
&\quad e^{i2\sigma\omega \sum_{p=1}^k (-1)^p \sum_{q=p}^k s_q - \omega\beta\Lambda(k)} \exp \left(-\sum_{p=1}^k \left(\sum_{q=p}^k s_q \right)^2 \right) \exp \left(\frac{k\beta^2}{4\sigma^2} - i\frac{\beta}{\sigma} (s_1 + 2s_2 + \cdots + ks_k) \right) ds_1 \cdots ds_k. \tag{C34}
\end{aligned}$$

With another change of variable $\tau_p = \sum_{q=p}^k s_q$, we obtain Eq. (C13). This concludes the proof.

3. Bounds of Term 1.1 and Term 1.2

In this section, we bound Term 1.1 and Term 1.2 separately so that the bound of Term 1 can be obtained by

$$\text{Term1} \leq \sum_{n \geq 1} \frac{(2\alpha\sigma^{1/2})^{2n}}{((2\pi)^{1/4})^{2n}} \|A_S\|^{2n} \sum_{\substack{k=0 \\ \text{even}}}^{2n} (\text{Term1,1} + \text{Term1,2}). \tag{C35}$$

We notice that Term 1.1 can be upper bounded by the inequality $|\sin(x)| \leq |x|$ as,

$$\begin{aligned} \text{Term 1.1} &= 2 \exp\left(\frac{(2n-k)\beta^2}{4\sigma^2}\right) \int_{-\infty < s_1 \leq s_2 \leq \dots \leq s_{2n-k} < \infty, -\infty < t_1 \leq t_2 \leq \dots \leq t_k < \infty} e^{-\sum_{p=1}^{2n-k} s_p^2 - \sum_{p=1}^k t_p^2} \\ &\quad \left| \int \gamma(\omega) e^{i2\sigma\omega \sum_{p=1}^{2n-k} (-1)^p s_p - i2\sigma\omega \sum_{p=1}^k (-1)^p t_p} d\omega \right| \left| \sin\left(\frac{\beta}{2\sigma} \sum_{p=1}^{2n-k} s_p\right) \right| ds_1 \dots ds_{2n-k} dt_1 \dots dt_k \\ &\leq \frac{\beta}{\sigma} \exp\left(\frac{(2n-k)\beta^2}{4\sigma^2}\right) \int_{-\infty < s_1 \leq s_2 \leq \dots \leq s_{2n-k} < \infty, -\infty < t_1 \leq t_2 \leq \dots \leq t_k < \infty} e^{-\sum_{p=1}^{2n-k} s_p^2 - \sum_{p=1}^k t_p^2} \\ &\quad \left| \int \gamma(\omega) e^{i2\sigma\omega \sum_{p=1}^{2n-k} (-1)^p s_p - i2\sigma\omega \sum_{p=1}^k (-1)^p t_p} d\omega \right| \left| \sum_{p=1}^{2n-k} s_p \right| ds_1 \dots ds_{2n-k} dt_1 \dots dt_k. \end{aligned} \quad (\text{C36})$$

Using the conditions on $\gamma(\omega)$ in Theorem 6, we obtain the following upper bound via integration by parts,

$$\left| \int \gamma(\omega) e^{i2\sigma\omega \sum_{p=1}^{2n-k} (-1)^p s_p - \sum_{p=1}^k (-1)^p t_p} d\omega \right| \leq \frac{1}{2\sigma} \frac{1}{|\sum_{p=1}^{2n-k} (-1)^p s_p - \sum_{p=1}^k (-1)^p t_p|} \int |\gamma'(\omega)| d\omega. \quad (\text{C37})$$

The goal becomes to prove the following integral is $\mathcal{O}(\frac{1}{\sigma})$. The integral can be separated as the summation of I and II,

$$\begin{aligned} &\int_{-\infty < s_1 \leq s_2 \leq \dots \leq s_{2n-k} < \infty, -\infty < t_1 \leq t_2 \leq \dots \leq t_k < \infty} e^{-\sum_{p=1}^{2n-k} s_p^2 - \sum_{p=1}^k t_p^2} \left| \int \gamma(\omega) e^{i2\sigma\omega \sum_{p=1}^{2n-k} (-1)^p s_p - \sum_{p=1}^k (-1)^p t_p} d\omega \right| \left| \sum_{p=1}^{2n-k} s_p \right| ds_1 \dots ds_{2n-k} dt_1 \dots dt_k \\ &= \int_{\substack{-\infty < s_1 \leq s_2 \leq \dots \leq s_{2n-k} < \infty, -\infty < t_1 \leq t_2 \leq \dots \leq t_k < \infty, \\ |\sum_{p=1}^{2n-k} (-1)^p s_p - \sum_{p=1}^k (-1)^p t_p| \geq \delta}} e^{-\sum_{p=1}^{2n-k} s_p^2 - \sum_{p=1}^k t_p^2} \\ &\quad \underbrace{\left| \int \gamma(\omega) e^{i2\sigma\omega \sum_{p=1}^{2n-k} (-1)^p s_p - \sum_{p=1}^k (-1)^p t_p} d\omega \right| \left| \sum_{p=1}^{2n-k} s_p \right| ds_1 \dots ds_{2n-k} dt_1 \dots dt_k}_\text{I} \\ &+ \int_{\substack{-\infty < s_1 \leq s_2 \leq \dots \leq s_{2n-k} < \infty, -\infty < t_1 \leq t_2 \leq \dots \leq t_k < \infty, \\ |\sum_{p=1}^{2n-k} (-1)^p s_p - \sum_{p=1}^k (-1)^p t_p| < \delta}} e^{-\sum_{p=1}^{2n-k} s_p^2 - \sum_{p=1}^k t_p^2} \\ &\quad \underbrace{\left| \int \gamma(\omega) e^{i2\sigma\omega \sum_{p=1}^{2n-k} (-1)^p s_p - \sum_{p=1}^k (-1)^p t_p} d\omega \right| \left| \sum_{p=1}^{2n-k} s_p \right| ds_1 \dots ds_{2n-k} dt_1 \dots dt_k}_\text{II}. \end{aligned} \quad (\text{C38})$$

To decouple the Fourier variable from the remaining Gaussian integrals, we introduce the following distance-preserving change of variables.

Lemma 10. *Given variables t_1, t_2, \dots, t_k , there exists an orthogonal matrix Q such that $\vec{t} = Q\vec{t}$, and*

$$t_1^2 + t_2^2 + \dots + t_k^2 = \tilde{t}_1^2 + \tilde{t}_2^2 + \dots + \tilde{t}_k^2, \quad \tilde{t}_1 = \sum_{p=1}^k (-1)^p t_p / \sqrt{k}. \quad (\text{C39})$$

This change of variable induces a change of integral area through \mathcal{T} , i.e., for a domain $D \subset \mathbb{R}^k$, its image is written $\mathcal{T}(D)$.

Proof. By Gram-Schmidt process, we can extend the vector $\left(\frac{-1}{\sqrt{k}}, \frac{1}{\sqrt{k}}, \dots, \frac{(-1)^k}{\sqrt{k}}\right)$ to the orthogonal matrix. \square

By Lemma 10, there exists orthogonal map Q_s, Q_t for the change of variable $\vec{s} = Q_s \vec{s}, \vec{t} = Q_t \vec{t}$ such that

$$\tilde{s}_1 = \sum_{p=1}^{2n-k} (-1)^p s_p / \sqrt{2n-k}, \quad \tilde{t}_1 = \sum_{p=1}^k (-1)^p t_p / \sqrt{k}. \quad (\text{C40})$$

Then,

$$I = \int_{\tilde{s}, \tilde{t}, |\sqrt{2n-k}\tilde{s}_1 - \sqrt{k}\tilde{t}_1| \geq \delta} e^{-\sum_{p=1}^{2n-k} \tilde{s}_p^2 - \sum_{p=1}^k \tilde{t}_p^2} \left| \int \gamma(\omega) e^{i2\sigma\omega(\sqrt{2n-k}\tilde{s}_1 - \sqrt{k}\tilde{t}_1)} d\omega \right| \left| \underbrace{(1, 1, \dots, 1)}_{2n-k} Q_S^T \tilde{s} \right| d\tilde{s}_1 \dots d\tilde{s}_{2n-k} d\tilde{t}_1 \dots d\tilde{t}_k. \quad (C41)$$

By Hölder and triangle inequality,

$$\left| \underbrace{(1, 1, \dots, 1)}_{2n-k} Q_S^T \tilde{s} \right| \leq \sqrt{2n-k} \left(|\tilde{s}_1| + \left(\sum_{p=2}^{2n-k} \tilde{s}_p^2 \right)^{1/2} \right). \quad (C42)$$

Combining this with the integration by parts, we have

$$\begin{aligned} I \leq & \sqrt{2n-k} \frac{1}{2\sigma} \int |\gamma'(\omega)| d\omega \int_{|\sqrt{2n-k}\tilde{s}_1 - \sqrt{k}\tilde{t}_1| \in (\delta, \infty)} e^{-(\tilde{s}_1^2 + \tilde{t}_1^2)} \frac{|\tilde{s}_1|}{|\sqrt{2n-k}\tilde{s}_1 - \sqrt{k}\tilde{t}_1|} d\tilde{s}_1 d\tilde{t}_1 \\ & \int_{\mathcal{T}(-\infty < s_2 \leq \dots \leq s_{2n-k} < \infty, -\infty < t_2 \leq \dots \leq t_k < \infty)} e^{-\sum_{p=2}^{2n-k} \tilde{s}_p^2 - \sum_{p=2}^k \tilde{t}_p^2} d\tilde{s}_2 \dots d\tilde{s}_{2n-k} d\tilde{t}_2 \dots d\tilde{t}_k \\ & + \sqrt{2n-k} \frac{1}{2\sigma} \int |\gamma'(\omega)| d\omega \int_{|\sqrt{2n-k}\tilde{s}_1 - \sqrt{k}\tilde{t}_1| \in (\delta, \infty)} e^{-(\tilde{s}_1^2 + \tilde{t}_1^2)} \frac{1}{|\sqrt{2n-k}\tilde{s}_1 - \sqrt{k}\tilde{t}_1|} d\tilde{s}_1 d\tilde{t}_1 \\ & \int_{\mathcal{T}(-\infty < s_2 \leq \dots \leq s_{2n-k} < \infty, -\infty < t_2 \leq \dots \leq t_k < \infty)} e^{-\sum_{p=2}^{2n-k} \tilde{s}_p^2 - \sum_{p=2}^k \tilde{t}_p^2} \left(\sum_{p=2}^{2n-k} \tilde{s}_p^2 \right)^{1/2} d\tilde{s}_2 \dots d\tilde{s}_{2n-k} d\tilde{t}_2 \dots d\tilde{t}_k. \end{aligned} \quad (C43)$$

Next, we perform the additional change of variable

$$\begin{cases} x = \sqrt{2n-k}\tilde{s}_1 - \sqrt{k}\tilde{t}_1 \\ y = \sqrt{k}\tilde{s}_1 + \sqrt{2n-k}\tilde{t}_1 \end{cases}, \quad (C44)$$

which gives

$$\begin{aligned} I \leq & \sqrt{2n-k} \frac{1}{2\sigma} \|\gamma'\|_{L^1} \frac{1}{2n} \int_{|x| \in (\delta, \infty)} e^{-\frac{x^2+y^2}{2n}} \frac{|\sqrt{2n-k}x + \sqrt{k}y|}{2n|x|} dx dy \\ & \int_{\mathcal{T}(-\infty < s_2 \leq \dots \leq s_{2n-k} < \infty, -\infty < t_2 \leq \dots \leq t_k < \infty)} e^{-\sum_{p=2}^{2n-k} \tilde{s}_p^2 - \sum_{p=2}^k \tilde{t}_p^2} ds_2 \dots ds_{2n-k} dt_2 \dots dt_k \\ & + \sqrt{2n-k} \frac{1}{2\sigma} \|\gamma'\|_{L^1} \frac{1}{2n} \int_{|x| \in (\delta, \infty)} e^{-\frac{x^2+y^2}{2n}} \frac{1}{|x|} dx dy \\ & \int_{\mathcal{T}(-\infty < s_2 \leq \dots \leq s_{2n-k} < \infty, -\infty < t_2 \leq \dots \leq t_k < \infty)} e^{-\sum_{p=2}^{2n-k} \tilde{s}_p^2 - \sum_{p=2}^k \tilde{t}_p^2} \left(\sum_{p=2}^{2n-k} \tilde{s}_p^2 \right)^{1/2} ds_2 \dots ds_{2n-k} dt_2 \dots dt_k. \end{aligned} \quad (C45)$$

By choosing $\delta = \mathcal{O}(1/\sigma)$, we have

$$\begin{aligned} & \int_{|x| \in (\delta, \infty)} e^{-\frac{x^2+y^2}{2n}} \frac{|\sqrt{2n-k}x + \sqrt{k}y|}{2n|x|} dx dy \leq \frac{\sqrt{2n-k}}{2n} \int_{|x| \in (\delta, \infty)} e^{-\frac{x^2+y^2}{2n}} dx dy + \frac{\sqrt{k}}{2n} \int_{|x| \in (\delta, \infty)} e^{-\frac{x^2+y^2}{2n}} \frac{|y|}{|x|} dx dy \\ & = \sqrt{2n-k}(\sqrt{\pi})^2 + \sqrt{k}\mathcal{O}\left(\log(\sqrt{2n}/\delta)\right) = \mathcal{O}\left(\sqrt{k}\log(\sqrt{2n}\sigma)\right), \end{aligned} \quad (C46)$$

and

$$\int_{|x| \in (\delta, \infty)} e^{-\frac{x^2+y^2}{2n}} \frac{1}{|x|} dx dy = \sqrt{2n}\mathcal{O}\left(\log(\sqrt{2n}/\delta)\right) = \sqrt{2n}\mathcal{O}\left(\log(\sqrt{2n}\sigma)\right). \quad (C47)$$

The remaining Gaussian integral can be upper bounded by the standard Gaussian bound. Using the change of variable

$x = \sum_{p=2}^{2n-k} \tilde{s}_p^2$ and the Gautschi's inequality, we obtain

$$\begin{aligned} & \int_{\mathcal{T}(-\infty < s_2 \leq \dots \leq s_{2n-k} < \infty, -\infty < t_2 \leq \dots \leq t_k < \infty)} e^{-\sum_{p=2}^{2n-k} \tilde{s}_p^2 - \sum_{p=2}^k \tilde{t}_p^2} \left(\sum_{p=2}^{2n-k} \tilde{s}_p^2 \right)^{1/2} ds_2 \dots ds_{2n-k} dt_2 \dots dt_k \\ & \leq (\sqrt{\pi})^{k-1} \int_0^\infty e^{-x} x^{\frac{2n-k-2}{2}} \frac{2\pi^{\frac{2n-k-1}{2}}}{\Gamma(\frac{2n-k-1}{2})} dx = 2 \frac{\Gamma(\frac{2n-k}{2})}{\Gamma(\frac{2n-k-1}{2})} \pi^{n-1} \leq 2 \sqrt{\frac{2n-k}{2}} \pi^{n-1}. \end{aligned} \quad (\text{C48})$$

and

$$\int_{\mathcal{T}(-\infty < s_2 \leq \dots \leq s_{2n-k} < \infty, -\infty < t_2 \leq \dots \leq t_k < \infty)} e^{-\sum_{p=2}^{2n-k} \tilde{s}_p^2 - \sum_{p=2}^k \tilde{t}_p^2} ds_2 \dots ds_{2n-k} dt_2 \dots dt_k \leq (\sqrt{\pi})^{2n}. \quad (\text{C49})$$

Consequently, combine those result together, we find

$$\begin{aligned} \text{I} & \leq \|\gamma'\|_{L^1} \frac{1}{\sigma} \frac{\sqrt{k(2n-k)}}{n} \pi^n \mathcal{O}(\log(\sqrt{2n}\sigma)) + \|\gamma'\|_{L^1} \frac{1}{\sigma} \frac{\sqrt{2n}(2n-k)}{n} \pi^n \mathcal{O}(\log(\sqrt{2n}\sigma)) \\ & \leq \|\gamma'\|_{L^1} \frac{(2\pi)^n}{\sigma} \mathcal{O}(\log(\sqrt{2n}\sigma)) \end{aligned} \quad (\text{C50})$$

We now turn to II. Using

$$\begin{aligned} & \int_{|x|<\delta} e^{-\frac{x^2+y^2}{2n}} \left| \frac{\sqrt{2n-k}}{2n} x + \frac{\sqrt{k}}{2n} y \right| dx dy \leq \frac{\sqrt{2n-k}}{2n} \int_{|x|<\delta} e^{-\frac{x^2+y^2}{2n}} |x| dx dy + \frac{\sqrt{k}}{2n} \int_{|x|<\delta} e^{-\frac{x^2+y^2}{2n}} |y| dx dy \\ & \leq \sqrt{(2n-k)/(2n)} \mathcal{O}(\delta^2) + \sqrt{k} \mathcal{O}(\delta). \end{aligned}$$

we have,

$$\begin{aligned} \text{II} & = \int_{-\infty < s_1 \leq s_2 \leq \dots \leq s_{2n-k} < \infty, -\infty < t_1 \leq t_2 \leq \dots \leq t_k < \infty, |\sum_{p=1}^{2n-k} (-1)^p s_p - \sum_{p=1}^k (-1)^p t_p| < \delta} e^{-\sum_{p=1}^{2n-k} s_p^2 - \sum_{p=1}^k t_p^2} \\ & \quad \left| \int \gamma(\omega) e^{i2\sigma\omega \sum_{p=1}^{2n-k} (-1)^p s_p - i2\sigma\omega \sum_{p=1}^k (-1)^p t_p} d\omega \right| \left| \sum_{p=1}^{2n-k} s_p \right| ds_1 \dots ds_{2n-k} dt_1 \dots dt_k \\ & \leq \int_{-\infty < s_1 \leq s_2 \leq \dots \leq s_{2n-k} < \infty, -\infty < t_1 \leq t_2 \leq \dots \leq t_k < \infty, |\sum_{p=1}^{2n-k} (-1)^p s_p - \sum_{p=1}^k (-1)^p t_p| < \delta} e^{-\sum_{p=1}^{2n-k} s_p^2 - \sum_{p=1}^k t_p^2} \left| \sum_{p=1}^{2n-k} s_p \right| ds_1 \dots ds_{2n-k} dt_1 \dots dt_k \\ & \leq \frac{1}{2n} \int_{|x|<\delta} e^{-\frac{x^2+y^2}{2n}} \left| \frac{\sqrt{2n-k}}{2n} x + \frac{\sqrt{k}}{2n} y \right| dx dy \int_{\mathcal{T}(-\infty < s_2 \leq \dots \leq s_{2n-k} < \infty, -\infty < t_2 \leq \dots \leq t_k < \infty)} e^{-\sum_{p=2}^{2n-k} \tilde{s}_p^2 - \sum_{p=2}^k \tilde{t}_p^2} d\tilde{s}_2 \dots d\tilde{s}_{2n-k} d\tilde{t}_2 \dots d\tilde{t}_k \\ & \quad + \frac{1}{2n} \int_{|x|<\delta} e^{-\frac{x^2+y^2}{2n}} dx dy \int_{\mathcal{T}(-\infty < s_2 \leq \dots \leq s_{2n-k} < \infty, -\infty < t_2 \leq \dots \leq t_k < \infty)} e^{-\sum_{p=2}^{2n-k} \tilde{s}_p^2 - \sum_{p=2}^k \tilde{t}_p^2} \sqrt{\sum_{p=2}^{2n-k} \tilde{s}_p^2} d\tilde{s}_2 \dots d\tilde{s}_{2n-k} d\tilde{t}_2 \dots d\tilde{t}_k \\ & \leq \left(\frac{\sqrt{(2n-k)/2n}}{2n} \mathcal{O}\left(\frac{1}{\sigma^2}\right) + \frac{\sqrt{k}}{n} \mathcal{O}\left(\frac{1}{\sigma}\right) \right) (\sqrt{\pi})^{2n-2} + \mathcal{O}\left(\frac{1}{\sigma}\right) (\sqrt{\pi})^k \\ & = \mathcal{O}\left(\pi^n \left(\frac{1}{n\sigma^2} + \frac{1}{\sqrt{n}\sigma}\right)\right) = \mathcal{O}\left(\frac{1}{\sqrt{n}\sigma} \pi^n\right) = \mathcal{O}\left(\frac{1}{n\sigma} (2\pi)^n\right). \end{aligned} \quad (\text{C51})$$

Putting everything together, we obtain

$$\text{Term 1.1} \leq \frac{\beta}{\sigma} \exp\left(\frac{(2n-k)\beta^2}{4\sigma^2}\right) (\text{I} + \text{II}) = \frac{\beta(2\pi)^n}{\sigma^2} \exp\left(\frac{(2n-k)\beta^2}{4\sigma^2}\right) \mathcal{O}\left(\|\gamma'\|_{L^1} \log(\sqrt{2n}\sigma) + \frac{1}{n}\right). \quad (\text{C52})$$

A similar argument yields an upper bound for Term 1.2,

$$\begin{aligned} \text{Term 1.2} &= \left| \exp \left(\frac{(2n-k)\beta^2}{4\sigma^2} \right) - 1 \right| \int_{\substack{-\infty < s_1 \leq s_2 \leq \dots \leq s_{2n-k} < \infty, \\ -\infty < t_1 \leq t_2 \leq \dots \leq t_k < \infty}} e^{-\sum_{p=1}^{2n-k} s_p^2 - \sum_{p=1}^k t_p^2} \\ &\quad \left| \int \gamma(\omega) e^{i2\sigma\omega \sum_{p=1}^{2n-k} (-1)^p s_p - i2\sigma\omega \sum_{p=1}^k (-1)^p t_p} d\omega \right| ds_1 \dots ds_{2n-k} dt_1 \dots dt_k \\ &\leq \frac{(2\pi)^n}{\sigma\sqrt{n}} \left| \exp \left(\frac{(2n-k)\beta^2}{4\sigma^2} \right) - 1 \right| \mathcal{O} \left(\log(\sqrt{2n}\sigma) \|\gamma'\|_{L^1} + \frac{\sqrt{n}}{\sigma} \right). \end{aligned} \quad (\text{C53})$$

Appendix D: Ground state preparation beyond Lindblad limit

For ground state preparation, we let the state of the environment be $\rho_E = |0\rangle\langle 0|$, we have the following result:

Theorem 11. (Ground state) Assume H has a spectral gap Δ and let $|\psi_0\rangle$ be the ground state of H . Then for any $\epsilon > 0$, if

$$\sigma = \Omega \left(\frac{1}{\Delta} \log^{3/2} (\|H\|/\epsilon) \right), \quad T = \tilde{\Omega}(\sigma), \quad \alpha = \mathcal{O} \left(\sigma^{-1/2} \right), \quad (\text{D1})$$

then

$$\|\Phi_\alpha(|\psi_0\rangle\langle\psi_0|) - |\psi_0\rangle\langle\psi_0|\|_1 < \alpha^2 \epsilon \quad (\text{D2})$$

To prove Theorem 11, we consider the zero temperature setting $\beta = \infty$. In which case, the evolution operator admits the following expression as $\beta \rightarrow \infty$,

$$\begin{aligned} \Phi_\alpha \rho_n &= \int g(\omega) \text{Tr}_E[U^\alpha(T)(\rho_n \otimes \rho_E)U^{\alpha\dagger}(T)](\omega) d\omega \\ &= U_S(2T)\rho_n U_S(2T)^\dagger \\ &\quad + \mathbb{E}_{A_S} \left(\sum_{n \geq 1} \alpha^{2n} (-1)^n \sum_{k=0}^{2n} (-1)^k \int_{-\infty}^0 (g(\omega) + g(-\omega)) U_S(T) G_{2n-k, A_S}^\dagger(\omega) U_S(T) \rho_n U_S^\dagger(T) G_{k, A_S}(\omega) U_S^\dagger(T) d\omega \right). \end{aligned} \quad (\text{D3})$$

We define the N finite summation as

$$\begin{aligned} \Phi_\alpha^N \rho_n &= U_S(2T)\rho_n U_S(2T)^\dagger \\ &\quad + \mathbb{E}_{A_S} \left(\sum_{n=1}^N \alpha^{2n} (-1)^n \sum_{k=0}^{2n} (-1)^k \int_{-\infty}^0 (g(\omega) + g(-\omega)) U_S(T) G_{2n-k, A_S}^\dagger(\omega) U_S(T) \rho_n U_S^\dagger(T) G_{k, A_S}(\omega) U_S^\dagger(T) d\omega \right). \end{aligned} \quad (\text{D4})$$

Then, the tail part can be bounded as:

$$\|\Phi_\alpha \rho_n - \Phi_\alpha^N \rho_n\|_1 \leq \sum_{n > N} \alpha^{2n} \sum_{k=0}^{2n} \|A_S\|^{2n} \sum_{k=0}^{2n} \frac{1}{(2n-k)!k!} \left(\int_{-\infty}^{\infty} f(t) dt \right)^{2n} = \sum_{n > N} \frac{(\mathcal{O}(\alpha \|A_S\| \sigma^{1/2}))^{2n}}{(2n)!} \quad (\text{D5})$$

In the following part of the proof, we assume A_S is a hermitian operator for simplicity. The calculation for the non-hermitian case is almost the same. We assume that there is a spectral gap $\Delta = \lambda_1 - \lambda_0 > 0$ of the system Hamiltonian H . This property can be utilized to show the decay property of the finite summation term by analyzing the Heisenberg picture system operator in the frequency space. The system Hamiltonian can be decomposed as

$$H = \sum_{\lambda_i \in \text{spec}(H)} \lambda_i |\psi_i\rangle\langle\psi_i|,$$

where the ground state $|\psi_0\rangle$ corresponds to the ground energy λ_0 . In the Heisenberg picture, any system operator A_S has the frequency space expansion,

$$A_S(t) = \sum_{i,j} e^{i(\lambda_i - \lambda_j)t} |\psi_i\rangle\langle\psi_i| A_S |\psi_j\rangle\langle\psi_j| = \sum_{\nu} e^{i\nu t} \sum_{\lambda_i - \lambda_j = \nu} |\psi_i\rangle\langle\psi_i| A_S |\psi_j\rangle\langle\psi_j| = \sum_{\nu \in B(H)} e^{i\nu t} A_S(\nu), \quad (\text{D6})$$

where $B(H) = \text{spec}(H) - \text{spec}(H)$ is the set of Bohr frequencies and

$$A_S(\nu) = \sum_{\lambda_i - \lambda_j = \nu} |\psi_i\rangle\langle\psi_i| A_S |\psi_j\rangle\langle\psi_j| . \quad (\text{D7})$$

Consequently,

$$A_S(t_1)A_S(t_2)\cdots A_S(t_n) = \sum_{\nu_1, \dots, \nu_n \in B(H)} e^{i\sum_{k=1}^n \nu_k t_k} A_S(\nu_1)A_S(\nu_2)\cdots A_S(\nu_n) . \quad (\text{D8})$$

Using the projection operator in Eq. (D7), the product of system operators on the frequency space follow

$$\begin{aligned} & A_S(\nu_1)A_S(\nu_2)\cdots A_S(\nu_n) \\ &= \sum_{E_k - E_{k+1} = \nu_k, k=1,2,\dots,n} |\psi_{E_1}\rangle\langle\psi_{E_1}| A_S |\psi_{E_2}\rangle\langle\psi_{E_2}| A_S \cdots |\psi_{E_n}\rangle\langle\psi_{E_n}| A_S |\psi_{E_{n+1}}\rangle\langle\psi_{E_{n+1}}| \end{aligned} \quad (\text{D9})$$

with $E_k \in \text{spec}(H)$. When substituting ρ_n into Eq. (D3) with the ground state $|\psi_0\rangle\langle\psi_0|$, it suffices to simplify the form of $\tilde{G}_{2n-k, A_S}^\dagger(\omega) |\psi_0\rangle$ and $\langle\psi_0| \tilde{G}_{k, A_S}(\omega)$ separately.

For $1 \leq n \leq N$, we have

$$\begin{aligned} \tilde{G}_{n, A_S}^\dagger(\omega) |\psi_0\rangle &= \int_{-\infty < s_1 \leq \dots \leq s_n < \infty} A_S(s_n) \cdots A_S(s_1) e^{i\omega \sum_{k=1}^n (-1)^k s_k} f(s_1) \cdots f(s_n) ds_1 \cdots ds_n |\psi_0\rangle \\ &= \int_{-\infty < s_n \leq \dots \leq s_1 < \infty} A_S(s_1) \cdots A_S(s_n) e^{i\omega \sum_{k=1}^n (-1)^{k+n+1} s_k} f(s_1) \cdots f(s_n) ds_1 \cdots ds_n |\psi_0\rangle \\ &= \sum_{\nu_1, \nu_2, \dots, \nu_n \in B(H)} \underbrace{\int_{-\infty}^{\infty} \cdots \int_{-\infty}^{s_{n-1}} f(s_1) \cdots f(s_n) \exp \left(i \sum_{k=1}^n (\nu_k + (-1)^{k+n+1} \omega) s_k \right) ds_n \cdots ds_1 A_S(\nu_1) \cdots A_S(\nu_n) |\psi_0\rangle}_{\text{I}_n(|\psi_0\rangle)} \\ &= \underbrace{\sum_{\sum_i \nu_i < \Delta} \int_{-\infty}^{\infty} \cdots \int_{-\infty}^{s_{n-1}} f(s_1) \cdots f(s_n) \exp \left(i \sum_{k=1}^n (\nu_k + (-1)^{k+n+1} \omega) s_k \right) ds_n \cdots ds_1 A_S(\nu_1) \cdots A_S(\nu_n) |\psi_0\rangle}_{\text{I}_n(|\psi_0\rangle)} \\ &+ \underbrace{\sum_{\sum_i \nu_i \geq \Delta} \int_{-\infty}^{\infty} \cdots \int_{-\infty}^{s_{n-1}} f(s_1) \cdots f(s_n) \exp \left(i \sum_{k=1}^n (\nu_k + (-1)^{k+n+1} \omega) s_k \right) ds_n \cdots ds_1 A_S(\nu_1) \cdots A_S(\nu_n) |\psi_0\rangle}_{\text{II}_n(|\psi_0\rangle)} \end{aligned} \quad (\text{D10})$$

For the first term, it can be rewritten using the projection operator in Eq. (D9) as

$$\begin{aligned} \text{I}_n(|\psi_0\rangle) &= \sum_{\sum_i \nu_i < \Delta} \int_{-\infty}^{\infty} \cdots \int_{-\infty}^{s_{n-1}} f(s_1) \cdots f(s_n) \exp \left(i \sum_{k=1}^n (\nu_k + (-1)^{k+n+1} \omega) s_k \right) ds_n \cdots ds_1 \\ &\quad \sum_{E_i - E_{i+1} = \nu_i, i=1,2,\dots,n} |\psi_{E_1}\rangle\langle\psi_{E_1}| A_S |\psi_{E_2}\rangle\langle\psi_{E_2}| A_S \cdots |\psi_{E_n}\rangle\langle\psi_{E_n}| A_S |\psi_{E_{n+1}}\rangle\langle\psi_{E_{n+1}}| |\psi_0\rangle \\ &= \sum_{\sum_i \nu_i < \Delta} \int_{-\infty}^{\infty} \cdots \int_{-\infty}^{s_{n-1}} f(s_1) \cdots f(s_n) \exp \left(i \sum_{k=1}^n (\nu_k + (-1)^{k+n+1} \omega) s_k \right) ds_n \cdots ds_1 \\ &\quad \sum_{E_i - E_{i+1} = \nu_i, i=1,2,\dots,n, E_1 - E_0 = \sum_i \nu_i < \Delta} |\psi_{E_1}\rangle\langle\psi_{E_1}| A_S |\psi_{E_2}\rangle\langle\psi_{E_2}| A_S \cdots |\psi_{E_n}\rangle\langle\psi_{E_n}| A_S |\psi_0\rangle . \end{aligned} \quad (\text{D11})$$

Since the Hamiltonian is gapped with $\Delta > 0$, every non-ground eigenvalue lies at least Δ above E_0 . Therefore, if the

accumulated energy input satisfies $E_1 - E_0 = \sum_{i=1}^n \nu_i < \Delta$, we must have $E_1 = E_0$ and

$$\begin{aligned} \text{I}_n(|\psi_0\rangle) &= \sum_{\sum_i \nu_i=0} \int_{-\infty}^{\infty} \cdots \int_{-\infty}^{s_{n-1}} f(s_1) \cdots f(s_n) \exp \left(i \sum_{k=1}^n (-1)^{k+n+1} \omega s_k \right) ds_n \cdots ds_1 \\ &\quad \left(\sum_{E_i-E_{i+1}=\nu_i, i=1,2,\cdots,n} \langle \psi_0 | A_S | \psi_{E_2} \rangle \langle \psi_{E_2} | A_S \cdots | \psi_{E_n} \rangle \langle \psi_{E_n} | A_S | \psi_0 \rangle \right) |\psi_0\rangle \\ &= \int_{-\infty}^{\infty} \cdots \int_{-\infty}^{s_{n-1}} f(s_1) \cdots f(s_n) \exp \left(i \sum_{k=1}^n (-1)^{k+n+1} \omega s_k \right) ds_n \cdots ds_1 \langle \psi_0 | A_S^n | \psi_0 \rangle |\psi_0\rangle = d_n |\psi_0\rangle, \end{aligned} \quad (\text{D12})$$

where

$$d_n := \int_{-\infty}^{\infty} \cdots \int_{-\infty}^{s_{n-1}} f(s_1) \cdots f(s_n) \exp \left(i \sum_{k=1}^n (-1)^{k+n+1} \omega s_k \right) ds_n \cdots ds_1 \langle \psi_0 | A_S^n | \psi_0 \rangle.$$

It reveals that the first term is always proportional to $|\psi_0\rangle$. From another side, the second term can be bounded as

$$\|\text{II}_n(|\psi_0\rangle)\| \leq \|A_S\|^n \sum_{\sum_i \nu_i \geq \Delta} \left| \int_{-\infty}^{\infty} \cdots \int_{-\infty}^{s_{n-1}} f(s_1) \cdots f(s_n) \exp \left(i \sum_{k=1}^n (\nu_k + (-1)^{k+n+1} \omega) s_k \right) ds_n \cdots ds_1 \right| \quad (\text{D13})$$

It is sufficient to calculate the multivariable Fourier transform of f .

Lemma 12 (Multivariable Fourier transformation of f).

$$\left| \int_{-\infty}^{\infty} \cdots \int_{-\infty}^{s_{n-1}} f(s_1) \cdots \exp \left(i \sum_{k=1}^n \alpha_k s_k \right) ds_n \cdots ds_1 \right| \leq (\mathcal{O}(\sigma^{1/2}))^n \frac{n^{n/2}}{n!} \exp \left(-\frac{\sigma^2}{n} \left(\sum_{k=1}^n \alpha_k \right)^2 \right) \quad (\text{D14})$$

Proof. We begin with change of variable $t_n = s_n$, $t_{n-1} = s_{n-1} - s_n$, $t_{n-2} = s_{n-2} - s_{n-1}$, \cdots , $t_1 = s_1 - s_2$ to partially decouple the multivariable Fourier transformation,

$$\begin{aligned} &\int_{-\infty}^{\infty} \cdots \int_{-\infty}^{s_{n-1}} f(s_1) \cdots \exp \left(i \sum_{k=1}^n \alpha_k s_k \right) ds_n \cdots ds_1 \\ &= \int_0^{\infty} \cdots \int_0^{\infty} \int_{-\infty}^{\infty} f \left(\sum_{k=1}^n t_k \right) f \left(\sum_{k=2}^n t_k \right) \cdots f(t_n) \exp \left(i \sum_{k=1}^n \left(\sum_{j=1}^k \alpha_j \right) t_k \right) dt_n \cdots dt_1. \end{aligned} \quad (\text{D15})$$

Substituting the expression of $f(t)$ back to the above expression, we obtain

$$\frac{1}{((2\pi)^{1/4} \sigma^{1/2})^n} \int_0^{\infty} \cdots \int_0^{\infty} \int_{-\infty}^{\infty} \exp \left(-\frac{1}{4\sigma^2} \sum_{k=1}^n \left(\sum_{p=k}^n t_p \right)^2 \right) \exp \left(i \sum_{p=1}^n \left(\sum_{k=1}^p \alpha_k \right) t_p \right) dt_n \cdots dt_1 \quad (\text{D16})$$

Notice that

$$\sum_{k=1}^n \left(\sum_{p=k}^n t_p \right)^2 = n \left(t_n + \frac{1}{n} \sum_{k=1}^{n-1} \sum_{p=k}^{n-1} t_p \right)^2 - \frac{1}{n} \left(\sum_{k=1}^{n-1} \sum_{p=k}^{n-1} t_p \right)^2 + \sum_{k=1}^{n-1} \left(\sum_{p=k}^{n-1} t_p \right)^2, \quad (\text{D17})$$

Eq. (D15) can be further simplified by calculating the inner integral with respect to t_n ,

$$\begin{aligned}
& \int_0^\infty \cdots \int_0^\infty \int_{-\infty}^\infty \exp\left(-\frac{n}{4\sigma^2}(t_n + \frac{1}{n} \sum_{k=1}^{n-1} \sum_{p=k}^{n-1} t_p)^2 + i \left(\sum_{k=1}^n \alpha_k\right) t_n\right) dt_n \\
& \exp\left(\frac{1}{4\sigma^2 n} \left(\sum_{k=1}^{n-1} \sum_{p=k}^{n-1} t_p\right)^2 - \frac{1}{4\sigma^2} \sum_{k=1}^{n-1} \left(\sum_{p=k}^{n-1} t_p\right)^2 + i \sum_{p=1}^{n-1} \left(\sum_{k=1}^p \alpha_k\right) t_p\right) dt_{n-1} \cdots dt_1 \\
& = \frac{2\sigma\sqrt{\pi}}{\sqrt{n}} \exp\left(-\frac{\sigma^2}{n} \left(\sum_{k=1}^n \alpha_k\right)^2\right) \int_0^\infty \cdots \int_0^\infty dt_{n-1} \cdots dt_1 \\
& \exp\left(\frac{1}{4\sigma^2 n} \left(\sum_{k=1}^{n-1} \sum_{p=k}^{n-1} t_p\right)^2 - \frac{1}{4\sigma^2} \sum_{k=1}^{n-1} \left(\sum_{p=k}^{n-1} t_p\right)^2 + i \sum_{p=1}^{n-1} \left(\sum_{k=1}^p \alpha_k\right) t_p - \frac{i}{n} \sum_{k=1}^n \alpha_k \sum_{k=1}^{n-1} \sum_{p=k}^{n-1} t_p\right).
\end{aligned} \tag{D18}$$

Thus, it can be upper bounded by the half line integral of decoupled Gaussian distribution,

$$\begin{aligned}
& \left| \int_0^\infty \cdots \int_0^\infty \int_{-\infty}^\infty \exp\left(-\frac{n}{4\sigma^2}(t_n + \frac{1}{n} \sum_{k=1}^{n-1} \sum_{p=k}^{n-1} t_p)^2 + i \sum_{k=1}^n \alpha_k t_n\right) dt_n \right. \\
& \left. \exp\left(\frac{1}{4\sigma^2 n} \left(\sum_{k=1}^{n-1} \sum_{p=k}^{n-1} t_p\right)^2 - \frac{1}{4\sigma^2} \sum_{k=1}^{n-1} \left(\sum_{p=k}^{n-1} t_p\right)^2 + i \sum_{p=1}^{n-1} \left(\sum_{k=1}^p \alpha_k\right) t_p\right) dt_{n-1} \cdots dt_1 \right| \\
& \leq \frac{2\sigma\sqrt{\pi}}{\sqrt{n}} \exp\left(-\frac{\sigma^2}{n} \left(\sum_{k=1}^n \alpha_k\right)^2\right) \int_0^\infty \cdots \int_0^\infty \exp\left(\frac{1}{4\sigma^2 n} \left(\sum_{k=1}^{n-1} \sum_{p=k}^{n-1} t_p\right)^2 - \frac{1}{4\sigma^2} \sum_{k=1}^{n-1} \left(\sum_{p=k}^{n-1} t_p\right)^2\right) dt_{n-1} \cdots dt_1 \\
& \leq \frac{2\sigma\sqrt{\pi}}{\sqrt{n}} \exp\left(-\frac{\sigma^2}{n} \left(\sum_{k=1}^n \alpha_k\right)^2\right) \int_0^\infty \cdots \int_0^\infty \exp\left(-\frac{1}{4\sigma^2 n} \sum_{k=1}^{n-1} \left(\sum_{p=k}^{n-1} t_p\right)^2\right) dt_{n-1} \cdots dt_1
\end{aligned} \tag{D19}$$

Notice that with another change of variable, $s_k = \sum_{p=k}^{n-1} t_p$, the nested integral can be calculated explicitly as

$$\begin{aligned}
& \int_0^\infty \cdots \int_0^\infty \exp\left(-\frac{1}{4\sigma^2 n} \sum_{k=1}^{n-1} \left(\sum_{p=k}^{n-1} t_p\right)^2\right) dt_{n-1} \cdots dt_1 = \int_{-\infty < s_1 \leq s_2 \leq \cdots \leq s_{n-1} < \infty} \exp\left(-\frac{1}{4\sigma^2 n} \sum_{k=1}^{n-1} s_k^2\right) ds_{n-1} \cdots ds_1 \\
& = \frac{1}{(n-1)!} \left(\int_{-\infty}^\infty \exp\left(-\frac{s^2}{4\sigma^2 n}\right) ds \right)^{n-1} = \frac{(2\sigma\sqrt{n\pi})^{n-1}}{(n-1)!}
\end{aligned} \tag{D20}$$

Combined with the above inequalities, we conclude the proof. \square

Replacing the Fourier coefficients in Lemma 12 with

$$\sum_{k=1}^n \alpha_k = \sum_{k=1}^n \nu_k + (-1)^{k+n+1} \omega = \begin{cases} \sum_{k=1}^n \nu_k & n \text{ is even} \\ \sum_{k=1}^n \nu_k - \omega & n \text{ is odd} \end{cases} \geq \Delta$$

as $\omega < 0$, we have

$$\begin{aligned}
\|\Pi_n(|\psi_0\rangle)\| & \leq \|A_S\|^n |B(H)|^n 2\sigma^{n/2} \pi^{n/4} \frac{n^{\frac{n}{2}-1}}{(n-1)!} \frac{1}{2^{n/4}} \exp\left(-\frac{\sigma^2}{n} \left(\sum_{k=1}^n \nu_k + (-1)^k \omega\right)^2\right) \\
& \leq \|A_S\|^n |B(H)|^n 2\sigma^{n/2} \pi^{n/4} \frac{n^{\frac{n}{2}-1}}{(n-1)!} \frac{1}{2^{n/4}} \exp\left(-\frac{\Delta^2 \sigma^2}{n}\right) \\
& = \frac{(\mathcal{O}(\|A_S\| |B(H)| \sigma^{1/2} n^{1/2}))^n}{n!} \exp\left(-\frac{\Delta^2 \sigma^2}{n}\right)
\end{aligned} \tag{D21}$$

For the finite dimension case, the Hamiltonian H can be approximated by H_η such that the eigenvalue are equal spaced with η and with the same ground state. One typical construction of H_η is

$$H_\eta = \sum_i g_\eta(\lambda_i) |\psi_i\rangle\langle\psi_i|, g_\eta(x) = \eta \left\lfloor \frac{x}{\eta} + \frac{1}{2} \right\rfloor. \tag{D22}$$

It induces $\|H - H_\eta\| \leq \eta$. Assume the above analysis are done with H_η , then $|B(H)| \leq \|H\|/\eta$, and

$$\begin{aligned} \|\Pi_n(|\psi_0\rangle)\| &\leq \|A_S\|^n \frac{\|H\|^n}{\eta^n} 2\sigma^{n/2} \pi^{n/4} \frac{n^{\frac{n}{2}-1}}{(n-1)!} \frac{1}{2^{n/4}} \exp\left(-\frac{\Delta^2 \sigma^2}{n}\right) \\ &= \frac{(\mathcal{O}(\|A_S\| \|H\| \eta^{-1} \sigma^{1/2} n^{1/2}))^n}{n!} \exp\left(-\frac{\Delta^2 \sigma^2}{n}\right) \end{aligned} \quad (\text{D23})$$

Additionally, by Duhamel's principle, $\|U_{S,H}(t) - U_{S,H_\eta}(t)\| \leq |t|\eta$, we have

$$\|U_{S,H}^\dagger(t)AU_{S,H}(t) - U_{S,H_\eta}^\dagger(t)AU_{S,H_\eta}(t)\| \leq 2\eta|t|\|A\|. \quad (\text{D24})$$

Thus, by multiplying them together,

$$\begin{aligned} &\|A_{S,H}(t_{k+1})A_{S,H}(t_{k+2}) \cdots A_{S,H}(t_{2n})|\psi_0\rangle\langle\psi_0|A_{S,H}(t_1) \cdots A_{S,H}(t_k) \\ &- A_{S,H_\eta}(t_{k+1})A_{S,H_\eta}(t_{k+2}) \cdots A_{S,H_\eta}(t_{2n})|\psi_0\rangle\langle\psi_0|A_{S,H_\eta}(t_1) \cdots A_{S,H_\eta}(t_k)\| \leq 2\eta\|A_S\|^{2n} \left(\sum_{i=1}^{2n} |t_i|\right) \end{aligned} \quad (\text{D25})$$

Define $G_{n,[\cdot],A_S}$ as the G operator with Hamiltonian $[\cdot]$ and A_S . Also, let the operator $\tilde{\Phi}_{\alpha,H_\eta}$ of the same form as in Eq. (C3), with only the Hamiltonian in the operator $G_{n,[\cdot],A_S}$ replaced with H_η ,

$$\tilde{\Phi}_{\alpha,H_\eta}(\rho) := U_{S,H}(T)\mathbb{E}_{A_S} \left(\sum_n \alpha^{2n} (-1)^n \sum_{k=0}^{2n} (-1)^k \int \gamma(\omega) \tilde{G}_{2n-k,H_\eta,A_S}^\dagger(\omega) U_{S,H}(T) \rho U_{S,H}^\dagger(T) \tilde{G}_{k,H_\eta,A_S}(\omega) d\omega \right) U_{S,H}^\dagger(T).$$

This inequality helps bound the difference between $\tilde{\Phi}_{\alpha,H}$ and $\tilde{\Phi}_{\alpha,H_\eta}$:

$$\begin{aligned} &\|\tilde{\Phi}_{\alpha,H}^N |\psi_0\rangle\langle\psi_0| - \tilde{\Phi}_{\alpha,H_\eta}^N |\psi_0\rangle\langle\psi_0|\|_1 \\ &\leq \mathbb{E}_{A_S} \left(\sum_{n=1}^N \alpha^{2n} \sum_{k=0}^{2n} \int_{-\infty}^0 (g(\omega) + g(-\omega)) \|U_{S,H}(T) \tilde{G}_{2n-k,H,A_S}^\dagger(\omega) U_{S,H}(T) |\psi_0\rangle\langle\psi_0| U_{S,H}^\dagger(T) \tilde{G}_{k,H,A_S}(\omega) U_{S,H}^\dagger(T) \right. \\ &\quad \left. - U_{S,H}(T) \tilde{G}_{2n-k,H_\eta,A_S}^\dagger(\omega) U_{S,H}(T) |\psi_0\rangle\langle\psi_0| U_{S,H}^\dagger(T) \tilde{G}_{k,H_\eta,A_S}(\omega) U_{S,H}^\dagger(T)\|_1 d\omega \right) \\ &\leq \mathbb{E}_{A_S} \left(\sum_{n=1}^N \alpha^{2n} \sum_{k=0}^{2n} \int_{-\infty}^0 (g(\omega) + g(-\omega)) \|\tilde{G}_{2n-k,H,A_S}^\dagger(\omega) |\psi_0\rangle\langle\psi_0| \tilde{G}_{k,H,A_S}(\omega) - \tilde{G}_{2n-k,H_\eta,A_S}^\dagger(\omega) |\psi_0\rangle\langle\psi_0| \tilde{G}_{k,H_\eta,A_S}(\omega)\|_1 d\omega \right) \\ &\leq \sum_{n=1}^N \alpha^{2n} \sum_{k=0}^{2n} 2\eta \|A_S\|^{2n} \int_{-\infty < t_{2n} \leq \cdots \leq t_{k+1} < \infty, -\infty < t_1 \leq \cdots \leq t_k < \infty} \left(\sum_{i=1}^{2n} |t_i| \right) f(t_1) \cdots f(t_{2n}) dt_1 \cdots dt_{2n} \\ &= \sum_{n=1}^N \alpha^{2n} \sum_{k=0}^{2n} 2\eta \|A_S\|^{2n} \frac{2n}{k!(2n-k)!} \left(\int_{-\infty}^\infty |t| f(t) dt \right) \left(\int_{-\infty}^\infty f(t) dt \right)^{2n-1} \\ &\leq 2\eta \sum_{n=1}^N \frac{(\alpha \|A_S\|)^{2n}}{(2n-1)!} \sum_{k=0}^{2n} \binom{2n}{k} \left(\frac{4\sigma^{3/2}}{(2\pi)^{1/4}} \right) \left(2^{3/4} \pi^{1/4} \sigma^{1/2} \right)^{2n-1} \\ &= \mathcal{O}(\eta \alpha^2 \sigma^2 \|A_S\|^2 \cosh(\mathcal{O}(\alpha \sigma^{1/2} \|A_S\|))). \end{aligned} \quad (\text{D26})$$

Notice $\alpha = \mathcal{O}(\sigma^{-1/2})$. We choose

$$\eta = \Theta(\sigma^{-2}\epsilon), \quad (\text{D27})$$

such that

$$\|\tilde{\Phi}_{\alpha,H}^N |\psi_0\rangle\langle\psi_0| - \tilde{\Phi}_{\alpha,H_\eta}^N |\psi_0\rangle\langle\psi_0|\|_1 = \mathcal{O}(\eta \alpha^2 (\sigma^2 + T\sigma) \|A_S\|^2 \cosh(\mathcal{O}(\alpha \sigma^{1/2} \|A_S\|))) \leq \frac{\alpha^2 \epsilon}{3}.$$

Now, we first show $\tilde{\Phi}_{\alpha,H_\eta}^N |\psi_0\rangle\langle\psi_0| \approx c |\psi_0\rangle\langle\psi_0|$. Given $N > 0$, we define

$$d_N = 1 + \sum_{n=1}^N \alpha^{2n} (-1)^n \sum_{k=0}^{2n} (-1)^k \int_{-\infty}^0 (g(\omega) + g(-\omega)) d_{2n-k}(\omega) d_k^*(\omega) d\omega \in \mathbb{R}. \quad (\text{D28})$$

We note that $d_0(\omega) = 1$ and

$$|d_{2n-k}| \leq \|A_S\|^{2n-k} \int_{-\infty < s_{2n-k} \leq \dots \leq s_1 < \infty} f(s_1) \cdots f(s_{2n-k}) ds_{2n-k} \cdots ds_1 = \frac{(\mathcal{O}(\|A_S\|\sigma^{1/2}))^{2n-k}}{(2n-k)!} \quad (\text{D29})$$

when $2n - k \geq 1$.

Combining this and Eq. (D23), we have

$$\begin{aligned} \left\| \tilde{\Phi}_{\alpha, H_\eta}^N |\psi_0\rangle\langle\psi_0| - d_N |\psi_0\rangle\langle\psi_0| \right\|_1 &\leq 2 \left\| \sum_{n=1}^N \alpha^{2n} (-1)^n \sum_{k=1}^{2n-1} (-1)^k \int_{-\infty}^0 (g(\omega) + g(-\omega)) d_{2n-k} |\psi_0\rangle \Pi_k^* (|\psi_0\rangle) d\omega \right\| \\ &+ \left\| \sum_{n=1}^N \alpha^{2n} (-1)^n \sum_{k=1}^{2n-1} (-1)^k \int_{-\infty}^0 (g(\omega) + g(-\omega)) \Pi_{2n-k} (|\psi_0\rangle) \Pi_k^* (|\psi_0\rangle) d\omega \right\| \\ &+ 2 \left\| \sum_{n=1}^N \alpha^{2n} (-1)^n \int_{-\infty}^0 (g(\omega) + g(-\omega)) \Pi_{2n} (|\psi_0\rangle) d\omega \right\| \\ &= \sum_{n=1}^N \left(\mathcal{O}(\alpha \|A_S\|\sigma^{1/2}) \right)^{2n} \sum_{k=1}^{2n} \frac{\|H\|^k k^{k/2}}{\eta^k k!(2n-k)!} \exp\left(-\frac{\sigma^2 \Delta^2}{k}\right) \\ &+ \sum_{n=1}^N \left(\mathcal{O}(\alpha \|A_S\|\sigma^{1/2}\|H\|\eta^{-1}) \right)^{2n} \sum_{k=1}^{2n-1} \frac{(2n-k)^{(2n-k)/2} k^{k/2}}{(2n-k)!(k)!} \exp\left(-\sigma^2 \Delta^2 \frac{2n}{k(2n-k)}\right) \\ &\leq \sum_{n=1}^N \left(\mathcal{O}(\|H\|\eta^{-1}) \right)^{2n} \sum_{k=1}^{2n} \frac{(2n-k)^{(2n-k)/2} k^{k/2}}{(2n-k)!(k)!} \exp\left(-\frac{\sigma^2 \Delta^2}{2n}\right) \end{aligned} \quad (\text{D30})$$

Here, the first and third terms in the initial inequality combine to produce the first term in the equality. In the last inequality, we use $\alpha = \mathcal{O}(\sigma^{-1/2})$ and $\|A_S\| \leq 1$.

Noticing that $\sum_{k=1}^{2n} \frac{(2n-k)^{(2n-k)/2} k^{k/2}}{(2n-k)!(k)!} \leq \frac{(\Theta(1))^n}{\sqrt{n!}}$. We obtain

$$\begin{aligned} &\sum_{n=1}^N \left(\mathcal{O}(\|H\|\eta^{-1}) \right)^{2n} \sum_{k=1}^{2n} \frac{(2n-k)^{(2n-k)/2} k^{k/2}}{(2n-k)!(k)!} \exp\left(-\frac{\sigma^2 \Delta^2}{2n}\right) \\ &= \sum_{n=1}^N \frac{\left(\mathcal{O}(\|H\|^2\eta^{-2}) \right)^n}{\sqrt{n!}} \exp\left(-\frac{\sigma^2 \Delta^2}{2n}\right) \\ &\leq \left(\max\{\mathcal{O}(\|H\|^2\eta^{-2}), 1\} \right)^N \sqrt{N} \exp\left(-\frac{\sigma^2 \Delta^2}{2N}\right) = \left(\mathcal{O}(\|H\|^2\sigma^4\epsilon^{-2}) \right)^N \sqrt{N} \exp\left(-\frac{\sigma^2 \Delta^2}{2N}\right) \end{aligned} \quad (\text{D31})$$

Plugging this back into (D30), we obtain

$$\left\| \tilde{\Phi}_{\alpha, H_\eta} |\psi_0\rangle\langle\psi_0| - d_N |\psi_0\rangle\langle\psi_0| \right\|_1 = \left(\mathcal{O}(\|H\|^2\sigma^4\epsilon^{-2}) \right)^N \sqrt{N} \exp\left(-\frac{\sigma^2 \Delta^2}{2N}\right),$$

Combine the above bounds with Theorem 7, we have

$$\begin{aligned} \|\Phi_{\alpha, H} |\psi_0\rangle\langle\psi_0| - |\psi_0\rangle\langle\psi_0| \|_1 &\leq \|\Phi_{\alpha, H} |\psi_0\rangle\langle\psi_0| - \tilde{\Phi}_{\alpha, H}^N |\psi_0\rangle\langle\psi_0| \|_1 + \|\tilde{\Phi}_{\alpha, H}^N |\psi_0\rangle\langle\psi_0| - \tilde{\Phi}_{\alpha, H} |\psi_0\rangle\langle\psi_0| \|_1 \\ &+ \|\tilde{\Phi}_{\alpha, H}^N |\psi_0\rangle\langle\psi_0| - \tilde{\Phi}_{\alpha, H_\eta}^N |\psi_0\rangle\langle\psi_0| \|_1 + \|\tilde{\Phi}_{\alpha, H_\eta}^N |\psi_0\rangle\langle\psi_0| - |\psi_0\rangle\langle\psi_0| \|_1 \\ &\leq \sum_{n>N}^{\infty} \frac{(\mathcal{O}(1))^{2n}}{2n!} + \mathcal{O}\left(\alpha^2 \sigma^2 \frac{1}{T} \exp\left(-\frac{T^2}{4\sigma^2}\right)\right) + \frac{\alpha^2 \epsilon}{3} + \left(\mathcal{O}(\|H\|^2\sigma^4\epsilon^{-2}) \right)^N \sqrt{N} \exp\left(-\frac{\sigma^2 \Delta^2}{2N}\right) \end{aligned} \quad (\text{D32})$$

Set $N = \Theta(\log(\alpha^{-1}\epsilon^{-1}))$, we have $\sum_{n>N}^{\infty} \frac{(\mathcal{O}(1))^{2n}}{2n!} < \frac{\alpha^2 \epsilon}{3}$. To make the last term smaller than $\alpha^2 \epsilon / 6$, it suffices to show

$$\exp\left(\frac{\sigma^2 \Delta^2}{2N}\right) \geq (\alpha^2 \epsilon)^{-1} \left(\mathcal{O}(\|H\|^2\sigma^4\epsilon^{-2}) \right)^N \sqrt{N}.$$

Recall $\alpha = \Theta(\sigma^{-1/2})$. This can be satisfied by choosing $\sigma = \Omega\left(\Delta^{-1} \log^{3/2}(\|H\|/\epsilon)\right)$. We conclude the proof.

Appendix E: Comparison with state preparation algorithm via Lindblad dynamics

In this section, we compare the complexity of system–bath interaction algorithm with the Lindblad-dynamics algorithm.

In [14], the authors demonstrate that, when $\alpha \ll 1$, (1) can be approximated by an effective Lindblad equation up to a unitary transformation. Let $U_S(t) = \exp(-itH)$ and $\mathcal{U}_S(t)[\rho] = U_S(t)\rho U_S^\dagger(t)$. They show that

$$\rho_{n+1} = \Phi_\alpha(\rho_n) = \mathcal{U}_S(T) \circ \exp(\mathcal{L}\alpha^2) \circ \mathcal{U}_S(T)[\rho_n] + \mathcal{O}(\alpha^4\sigma^2). \quad (\text{E1})$$

Here, \mathcal{L} is a Lindbladian operator that takes the form of

$$\mathcal{L}(\rho) = -i[H_{\text{LS}}, \rho] + \underbrace{\mathbb{E}_{A_S} \left(\int_{-\infty}^{\infty} \gamma(\omega) \mathcal{D}_{V_{A_S,f,T}(\omega)}(\rho) d\omega \right)}_{:=\mathcal{L}_D}, \quad (\text{E2})$$

where H_{LS} is a Lamb-shift Hamiltonian and

$$\mathcal{D}_{V_{A_S,f,T}(\omega)}(\rho) = V_{A_S,f,T}(\omega)\rho V_{A_S,f,T}(\omega)^\dagger - \frac{1}{2}\{V_{A_S,f,T}(\omega)^\dagger V_{A_S,f,T}(\omega), \rho\}, \quad V_{A_S,f,T}(\omega) = \int_{-T}^T f(t)A_S(t) \exp(-i\omega t) dt.$$

Assuming \mathcal{L} has a contraction mixing time $t_{\text{mix},\mathcal{L}}$, i.e., for any density states ρ_1, ρ_2 ,

$$\|\exp(\mathcal{L}t_{\text{mix},\mathcal{L}})[\rho_1] - \exp(\mathcal{L}t_{\text{mix},\mathcal{L}})[\rho_2]\|_1 \leq \frac{1}{2}\|\rho_1 - \rho_2\|_1.$$

Define $\tau_\alpha = \lceil t_{\text{mix},\mathcal{L}}/\alpha^2 \rceil$. By choosing α to be sufficiently small so that $\alpha\sqrt{\sigma} = \mathcal{O}(1)$, we have

$$\|\Phi_\alpha^{\tau_\alpha}(\rho_1) - \Phi_\alpha^{\tau_\alpha}(\rho_2)\|_1 \leq \left(\frac{1}{2} + \mathcal{O}(\alpha^4\sigma^2) \right) \|\rho_1 - \rho_2\|_1 \leq \frac{3}{4}\|\rho_1 - \rho_2\|_1.$$

This implies that, when α is chosen according to Theorem 2 or Theorem 3 ($\alpha\sqrt{\sigma} = \Theta(1)$), the integer mixing time of the channel Φ_α scales as

$$\tau_{\text{mix},\Phi_\alpha} = \Theta(\tau_\alpha) = \Theta\left(\frac{t_{\text{mix},\mathcal{L}}}{\alpha^2}\right) = \Theta(t_{\text{mix},\mathcal{L}}\sigma).$$

This is the number of repetitions of the quantum channel Φ_α required to prepare the steady state of the system. Because $T = \tilde{\Theta}(\sigma)$ according to Theorem 2 and Theorem 3, the total evolution time of the system Hamiltonian H scales as

$$T_{\text{total},\Phi_\alpha} = \tau_{\text{mix},\Phi_\alpha} \cdot 2T = \tilde{\Theta}(t_{\text{mix},\mathcal{L}}\sigma^2). \quad (\text{E3})$$

It is worth noting that although $\tau_{\text{mix},\Phi_\alpha}$ can be upper bounded via the perturbation argument under the scaling $\alpha\sqrt{\sigma} = \Theta(1)$, the analysis in [14] does not provide a rigorous guarantee on the steady-state error in this regime. The reason is that the perturbation error $\mathcal{O}(\alpha^4\sigma^2)$ in (E1) does not vanish as $\alpha \rightarrow 0$ under the scaling $\alpha\sqrt{\sigma} = \Theta(1)$, and therefore the perturbation argument used in [14] no longer applies. Nevertheless, our theoretical analysis shows that high-accuracy thermal and ground state preparation can still be achieved under this scaling.

We now compare our approach with the Lindblad-dynamics algorithm studied in the literature. The operator \mathcal{L}_D in (E2) was proposed as a Lindbladian for the state preparation in [6] and the algorithm simulates the dynamics:

$$\partial_t \rho = \mathcal{L}_D(\rho). \quad (\text{E4})$$

Furthermore, assuming the Lindbladian \mathcal{L}_D has a contraction mixing time $t_{\text{mix},\mathcal{L}_D}$, the total evolution time of the system Hamiltonian H for preparing the thermal state as [6, Theorem I.2] scales as

$$T_{\text{total},\mathcal{L}_D} = \tilde{\Theta}(t_{\text{mix},\mathcal{L}_D}\sigma).$$

Assuming $t_{\text{mix},\mathcal{L}_D} = \Theta(t_{\text{mix},\mathcal{L}})$, the above calculation shows that the system–bath–interaction algorithm is approximately a factor of σ more expensive than the Lindblad-dynamics algorithm for thermal state preparation. In the case of thermal state preparation, it was shown in [6, 14] that both dynamics require $\sigma = \tilde{\Theta}(\beta\epsilon^{-1}t_{\text{mix}})$ to achieve a target

precision ϵ . Therefore, the system–bath–interaction algorithm has a total Hamiltonian evolution time larger than that of the Lindblad-dynamics algorithm by a factor of $\tilde{\Theta}(\beta\epsilon^{-1}t_{\text{mix}})$. In the case of ground state preparation [33], as shown in [14], it suffices to choose $\sigma = \tilde{\Theta}(\Delta^{-1})$, where Δ is the spectral gap of the Hamiltonian H . Thus, in this case, the system–bath–interaction algorithm has a total Hamiltonian evolution time larger than that of the Lindblad-dynamics algorithm only by a factor of $\tilde{\Theta}(\Delta^{-1})$.

Although the complexity of the system–bath–interaction algorithm appears to be higher than that of the Lindblad-dynamics algorithm based on the above comparison according to our theoretical bounds, further improvements and a more refined analysis may reduce this gap. We highlight several important points below:

- In the above comparison, we fixed $\alpha\sqrt{\sigma} = \Theta(1)$ in accordance with the theoretical guarantees established in this paper. However, as shown in our numerical experiments in Appendix F 1, high-accuracy thermal and ground state preparation can still be achieved even when $\alpha\sqrt{\sigma} = \Theta(1)$, and in this regime the mixing time $\tau_{\text{mix},\Phi_\alpha}$ continues to scale as α^{-2} . If $\alpha\sqrt{\sigma} = \Theta(1)$, the system–bath–interaction algorithm can be further accelerated, reducing the total Hamiltonian evolution time, and the resulting overhead matches the scaling of the Lindblad-dynamics algorithm.
- In the above calculation, we assumed that $t_{\text{mix},\mathcal{L}_D} = \Theta(t_{\text{mix},\mathcal{L}})$. While this equivalence can be verified for certain physical models in the small- σ regime, as shown in [14], establishing it rigorously in full generality remains an open problem. In particular, a deeper understanding is needed of how the Lamb-shift term H_{LS} influences the mixing time.
- It is worth noting that, for thermal state preparation, the dynamics in Eq. (E4) is not the current state of the art. Recent works [7, 11] have proposed refined Lindblad generators that incorporate a correction Hamiltonian chosen to enforce the exact KMS detailed balance condition. This modification reduces the required value of σ from $\beta\epsilon^{-1}t_{\text{mix}}$ to $\beta\log(t_{\text{mix}}/\epsilon)$, yielding a substantial improvement. It is an interesting open direction to investigate whether analogous corrections can be implemented in the system–bath–interaction framework, potentially leading to a similar reduction in the total Hamiltonian evolution time.

Appendix F: Detailed numerical implementation

We consider the transverse field Ising model (TFIM) and the Hubbard model to testify our algorithm.

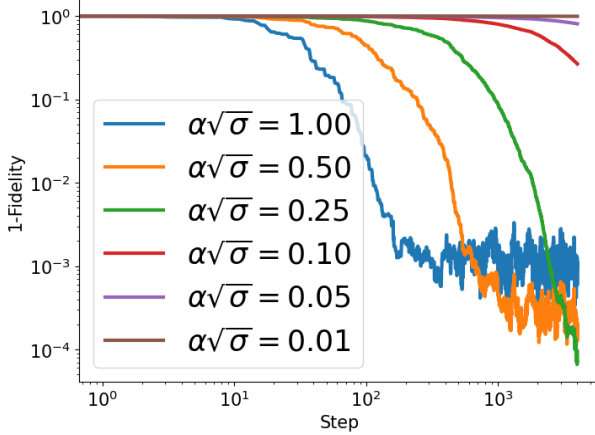
1. Transverse field Ising model (TFIM)

Recall the transverse field Ising model (TFIM) in (4):

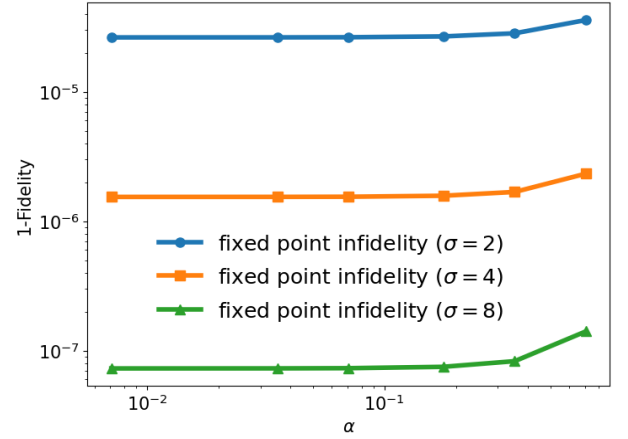
$$H = -J \sum_{i=1}^{L-1} Z_i Z_{i+1} - g \sum_{i=1}^L X_i,$$

where we set $J = 1, g = 1.2$. We now provide more detailed numerical results for both thermal state and ground state preparation with different choices of parameters.

- The thermal state setting with $L = 4$: The additional numerical results are presented in Fig. 4. As shown in Fig. 4a, the state converges to the thermal state with very high accuracy, and the convergence rate improves as α increases. Moreover, Fig. 4b illustrates that the steady state of the channel approaches the target thermal state as σ increases, while remaining nearly constant with respect to variations in α .
- The ground state setting with $L = 4$: we set $\alpha = 0.5, 0.25, 0.125, 0.05, 0.025, 0.005$, $\sigma = 4, 8, 16$, $T = 5\sigma$, and also sample ω uniformly from $[0, 5]$. The results are shown in Fig. 5. Similar to the thermal state case, figures in Fig. 5a and Fig. 5b justifies the convergence behavior of the fidelity and energy in the algorithm. More detailed numerical tests and similar results as the thermal state case are presented in Fig. 5c and Fig. 5d.
- Strong coupling regime with $L = 4$: We extend our numerical experiments to the regime where $\alpha\sqrt{\sigma} = \Theta(1)$. For thermal state preparation, we keep σ , T , and ω the same as before and vary α as $\alpha/\sqrt{2} = 1, 0.5, 0.25, 0.1, 0.05, 0.01$. For ground state preparation, we again fix all other parameters and choose $\alpha = 2, 1, 0.5, 0.2, 0.1, 0.02$. The results are shown in Fig. 6. For both thermal and ground states, we observe that when $\alpha/\sqrt{\sigma} \leq 1/2$, the fixed point remains close to the target state, and the spectral gap continues to scale as α^2 in this regime. These observations suggest that accurate thermal and ground state preparation remains feasible even under strong system–bath interactions, with a correspondingly faster convergence rate.

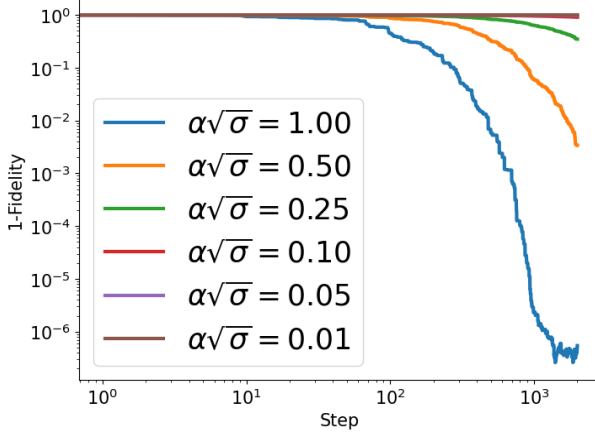


(a) The evolution of infidelity. Here, we set $\sigma = 2$ and $\alpha\sqrt{\sigma}$.

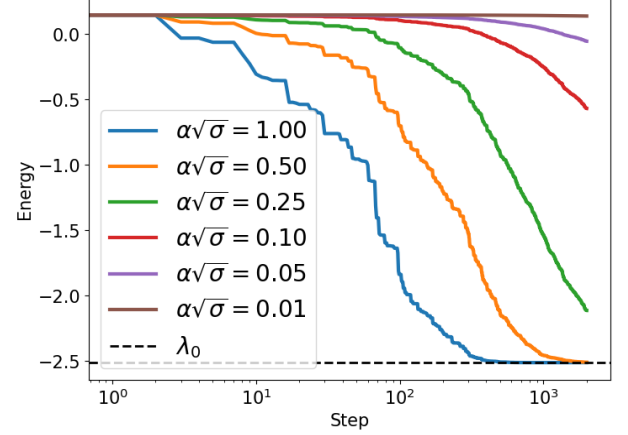


(b) Infidelity between target thermal state and the stationary state of Φ_α with different σ .

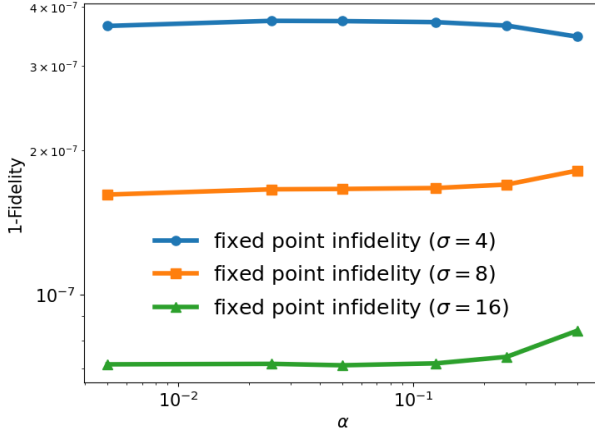
Figure 4: TFIM-4 with $\alpha\sqrt{\sigma} = \Omega(1)$ and $\beta = 1$.



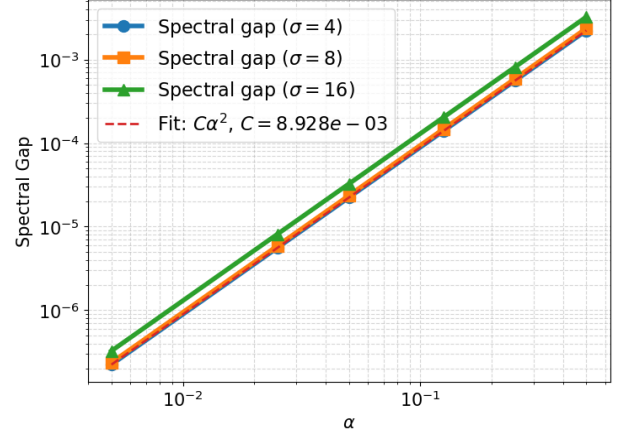
(a) The evolution of 1-fidelity. Here, we set $\sigma = 4$ and $\alpha\sqrt{\sigma}$.



(b) The evolution of energy. Here, λ_0 is the ground state energy and we set $\sigma = 2$ and $\alpha\sqrt{\sigma}$.

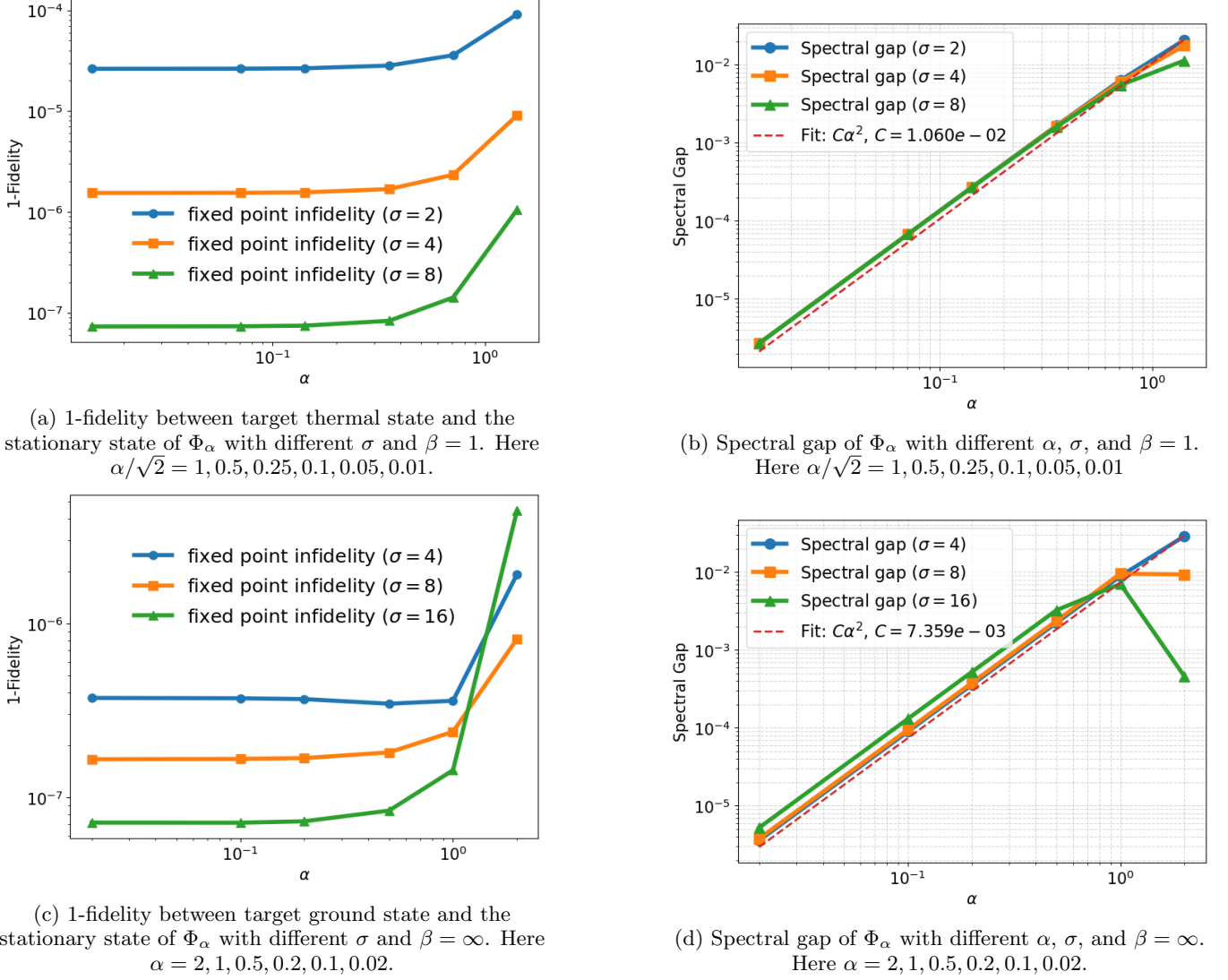


(c) 1-fidelity between target thermal state and the stationary state of Φ_α with different σ . Fidelity increases with σ . Here, $\alpha = 0.5, 0.25, 0.125, 0.05, 0.025, 0.005$.



(d) Spectral gap of Φ_α with different α and σ . The spectral gap scales as α^2 and is independent of σ . Here, $\alpha = 0.5, 0.25, 0.125, 0.05, 0.025, 0.005$.

Figure 5: TFIM-4 with $\alpha\sqrt{\sigma} = \Omega(1)$ and $\beta = \infty$.

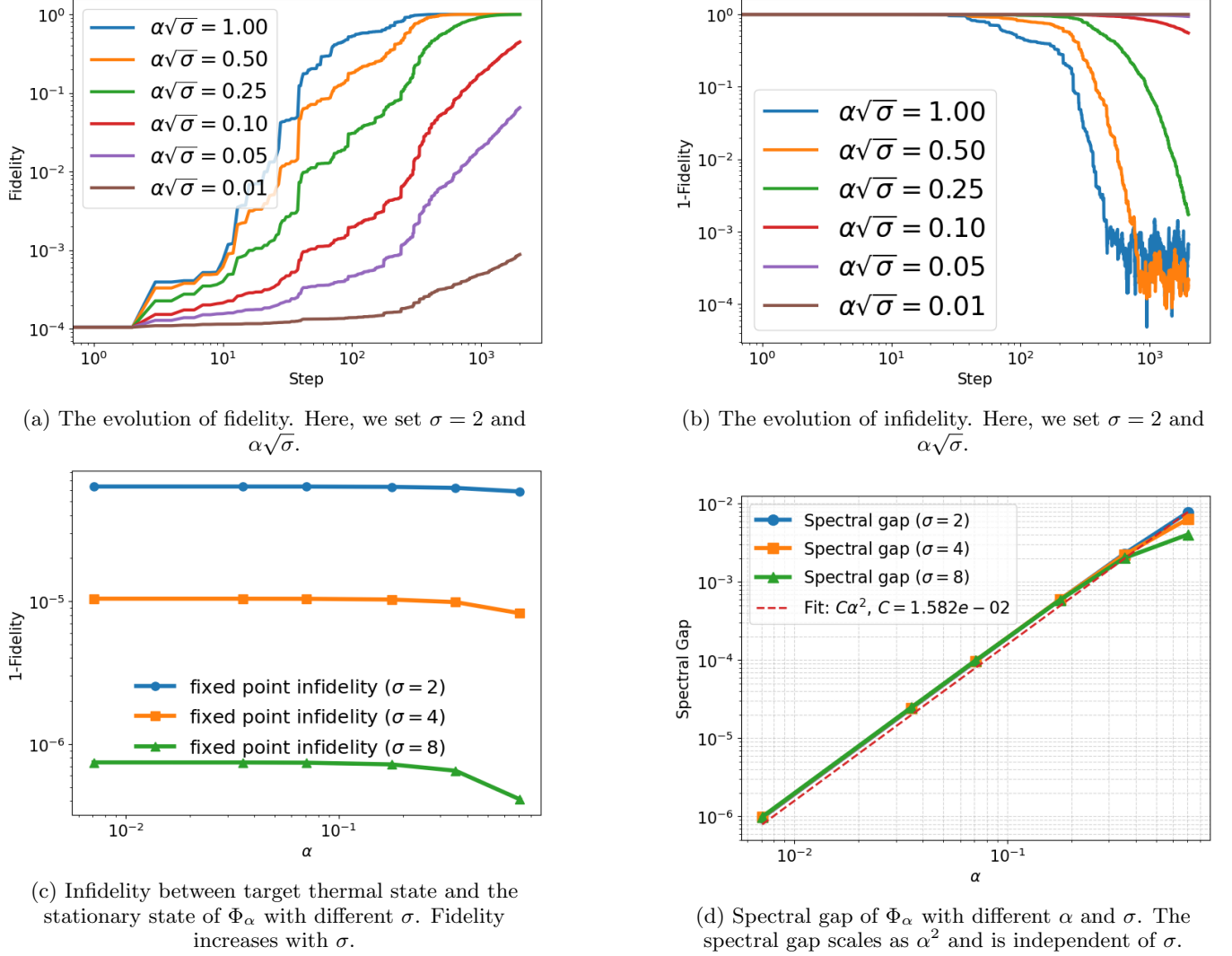
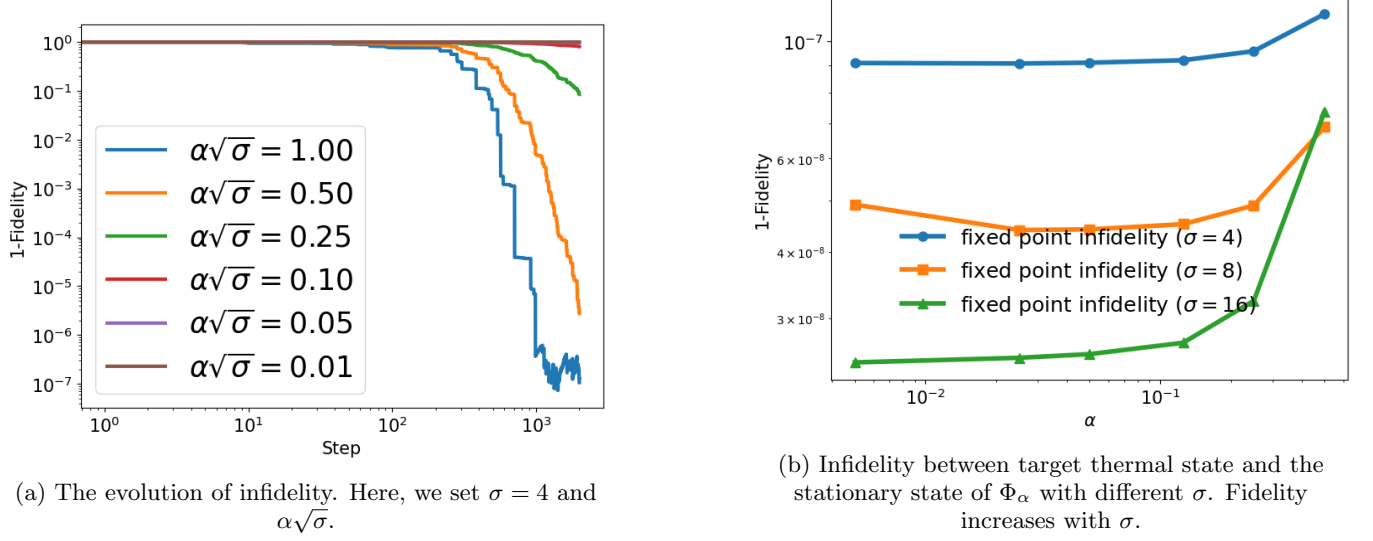
Figure 6: TFIM-4 with $\alpha/\sqrt{\sigma} = \Omega(1)$.

2. 1-D Hubbard model

Recall the 1-D Hubbard model defined in (5):

$$H = -t \sum_{j=1}^{L-1} \sum_{\sigma \in \{\uparrow, \downarrow\}} c_{j,\sigma}^\dagger c_{j+1,\sigma} + U \sum_{j=1}^L (n_{j,\uparrow} - \frac{1}{2})(n_{j,\downarrow} - \frac{1}{2})$$

where we choose $t = 1, U = -4$. Similar to the TFIM case, we consider both the thermal state and the ground state case with the same choice of parameters. We observe very similar results in Fig. 7 and Fig. 8. Furthermore, the numerical experiments can be extended to the regime where $\alpha/\sqrt{\sigma} = \mathcal{O}(1)$, as shown in Fig. 9. Similar to the TFIM-4 case, when $\alpha/\sqrt{\sigma} \leq 1/2$, the fixed point closely matches the target state, and the spectral gap increases as α^2 .

Figure 7: Hubbard-2 with $\alpha\sqrt{\sigma} = \Omega(1)$ and $\beta = 1$.Figure 8: Hubbard-2 with $\alpha\sqrt{\sigma} = \Omega(1)$ and $\beta = \infty$.

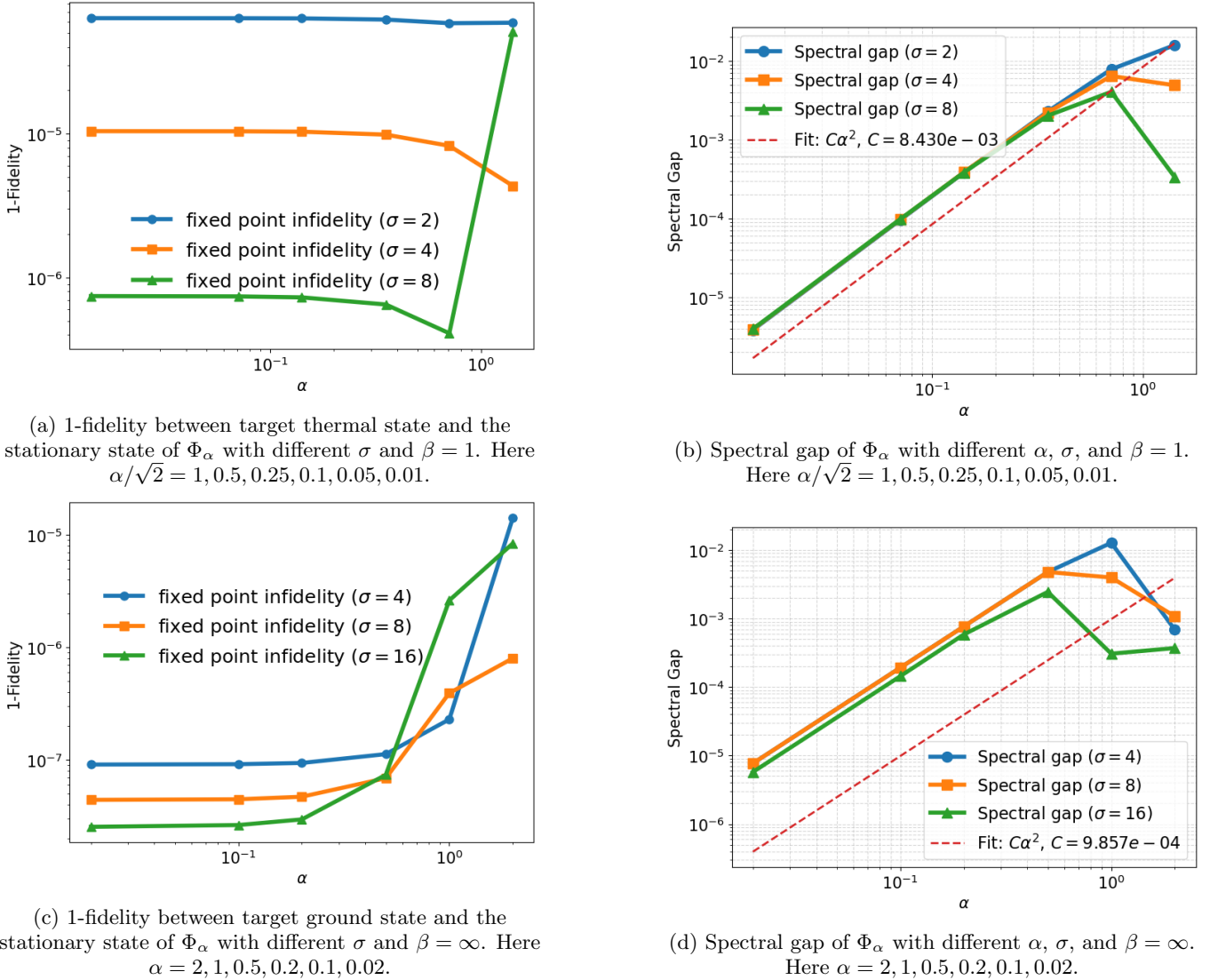


Figure 9: Hubbard-2 with $\alpha/\sqrt{\sigma} = \Omega(1)$.

3. ANNNI model

Consider the 1-D axial next-nearest-neighbor Ising (ANNNI) model defined as

$$H_{\text{ANNNI}} = \frac{J_1}{4} \sum_i Z_i Z_{i+1} + \frac{J_2}{4} \sum_i Z_i Z_{i+2} - \frac{\Gamma}{2} \sum_i X_i, \quad (\text{F1})$$

with $J_1 = 2$, $J_2 = 0.6$, $\Gamma = 0.2$, and $\rho_0 = |0\rangle\langle 0|$. In our test, we set the number of sites $L = 4$, $\alpha = 2, 1, 0.5, 0.2, 0.1, 0.02$, $\sigma = 4, 8, 16$, and $T = 5\sigma$. The result is shown in Fig. 10. Similar to the TFIM and Hubbard models, our algorithm converges to the correct ground state whenever $\alpha/\sqrt{\sigma} \leq \frac{1}{2}$, and the convergence rate increases proportionally to α^2 .

4. Ground state preparation with 8 qubits

We also consider the ground state preparation of TFIM and Hubbard model with 8 qubits, i.e. TFIM-8 and Hubbard-4, respectively. The results are shown in Fig. 11. Different from previous numerical experiments, we test the evolution of state vector instead of density operator to reduce the computational cost. Thus, we only present the evolution of energy along a single trajectory. The parameters are the same as before. Similar to the thermal state

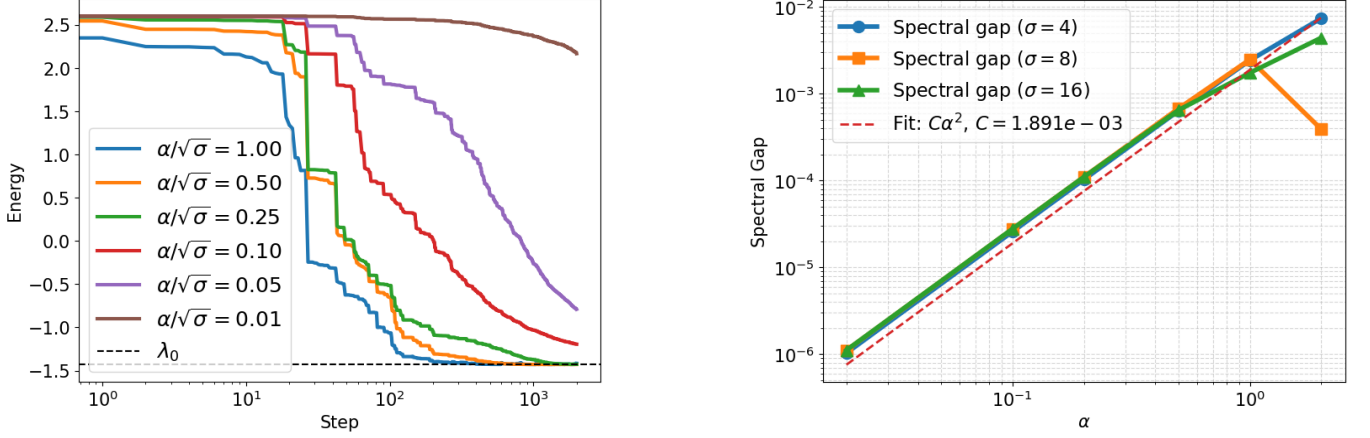


Figure 10: Ground state preparation for ANNNI model $\alpha/\sqrt{\sigma} = \Theta(1)$. Left: Evolution of energy, λ_0 is the ground state energy; Right: Spectral gap with different σ .

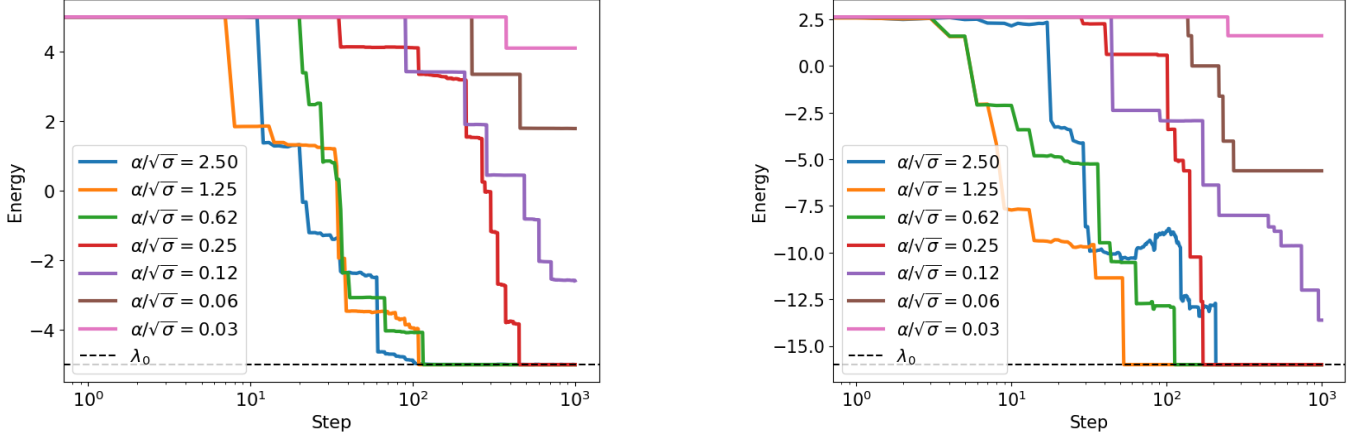


Figure 11: Evolution of energy for ground state with $\alpha/\sqrt{\sigma} = \Theta(1)$, λ_0 is the ground state energy. Left: TFIM with $L = 8$ sites; Right: Hubbard model with $L = 4$ sites.

case, even in the strong-coupling regime ($\alpha/\sqrt{\sigma} \approx 0.5$), the algorithm still converges to the ground state with high accuracy, and the convergence speed increases as α grows.